

## Pseudotetragonal and orthorhombic ordered structures in substoichiometric $\text{YBa}_2\text{Cu}_3\text{O}_{6+x}$ oxides at $x < 0.4$

S. Semenovskaya and A. G. Khachatryan

*Department of Materials Science, Rutgers University, P.O. Box 909, Piscataway, New Jersey 08855-0909*

(Received 14 July 1994; revised manuscript received 22 November 1994)

The previous analysis [S. Semenovskaya and A.G. Khachatryan, *Phys. Rev. B* **46**, 6511 (1992); *Physica D* **66**, 205 (1993)] of the structural transformations in nonstoichiometric  $\text{YBa}_2\text{Cu}_3\text{O}_{6+x}$  oxides is extended to a "tetragonal" stoichiometry region,  $x < 0.4$ . Available diffraction data [Th. Zeiske, D. Hohlwein, R. Sonntag, F. Kubanek, and G. Collin, *Z. Phys. B* **86**, 11 (1992); Tan Kemin, Hu Meisheng, and W. Yening, *J. Phys. Condens. Matter* **1**, 1049 (1989)] (on the  $\sqrt{2}a_0 \times 2\sqrt{2}a_0$  structures formed at small  $x < 0.4$ ) are analyzed by the concentration-wave method and computer-simulation technique. It is found that at small  $x < 0.4$ , oxygen ordering results in a sequence of transformations different from those observed at  $x > 0.5$ . It produces the pseudotetragonal and orthorhombic  $\{\frac{1}{4}\frac{1}{4}0\}$  phases formed by the  $(\frac{1}{2}\frac{1}{2}0)$  and  $\{\frac{1}{4}\frac{1}{4}0\}$  concentration waves. These phases form a family of  $[110]$  oxygen-atom chain structures, which are different from the  $[010]$  Cu(1)-O chain structures formed at  $x > 0.5$ . These differences can be explained only if a significant change in oxygen-oxygen (O-O) potential near  $x \sim 0.4$  (where the superconductivity disappears) is assumed. The O-O interaction potential at  $x < 0.4$  was estimated and used to perform computer simulations of oxygen ordering kinetics at  $x = 0.25$ .

### I. INTRODUCTION

In spite of numerous studies of the ordered phases in  $\text{YBa}_2\text{Cu}_3\text{O}_{6+x}$  high-temperature superconductors, there is still no convincing evidence that the  $\text{YBa}_2\text{Cu}_3\text{O}_{6+x}$  system undergoes a decomposition into a mixture of ordered phases to maintain the stoichiometric composition at low temperatures, as it is required by the third law of thermodynamics. This behavior may be expected if the interaction between oxygen atoms is a repulsive long-range Coulomb-like interaction. When the decomposition mechanism is not operative, the stoichiometry  $x$  can be only reached by a series of the consecutive congruent ordering reactions, adjusting the ideal stoichiometry of the resultant ordered phases to the current stoichiometry  $x$ . In this respect, the congruent multiple ordering of oxygen seems to be the only feasible alternative to the decomposition. Therefore, we can expect a large variety of ordered phases in this system, especially rich at low temperatures.

The superconducting properties of the  $\text{YBa}_2\text{Cu}_3\text{O}_{6+x}$  oxides are known to be closely related to the oxygen ordering in the  $(001)$  Cu(1)-O basal planes resulting in formation of the Cu-O chain structures along the  $[010]$  direction. They are the orthorhombic O-I and double-period O-II ordered phases formed from the disordered tetragonal  $T$  phase. The diffraction data indicate that besides these two phases small domains of the  $[010]$  chain structures with an  $na_0 \times a_0$  unit cell ( $a_0$  is the perovskite lattice parameter,  $n = 3-5$ ) may also be formed.<sup>4-8</sup>

However, even the earliest electron-diffraction studies of nonstoichiometric  $\text{YBa}_2\text{Cu}_3\text{O}_{6+x}$  oxides found the structures which are not the  $[010]$  chain structures. They generate the  $\{\frac{1}{4}\frac{1}{4}0\}$ -type superlattice diffraction maxima and are generally referred to as the  $2\sqrt{2}a_0 \times 2\sqrt{2}a_0$

phases.<sup>7,9-12</sup> It is interesting that the recent neutron-<sup>13</sup> and the x-rays-<sup>2</sup> diffraction studies of the oxide with  $x = 0.35$  found new  $\{\frac{1}{4}\frac{1}{4}0\}$  phases which substantially differ from the previously discovered ones. Figure 1 schematically shows three different diffraction patterns with the  $\{\frac{1}{4}\frac{1}{4}0\}$ -type superlattice diffraction maxima that were observed for the structures named below as the  $\{\frac{1}{4}\frac{1}{4}0\}$  phases. Figure 1(a) illustrates a recently found new type of diffraction pattern obtained by Zeiske *et al.*<sup>2</sup> by x-ray diffraction from a tiny crystal with domains of one orientation (the sample of  $\text{YBa}_2\text{Cu}_3\text{O}_{6.35}$  had  $x = 0.35$ ). The same diffraction pattern was observed earlier by Kemin *et al.*<sup>3</sup> Actually, the last study received two types of diffractions, shown in Figs. 1(a) and 1(b), although the difference between them was not underlined in this work. The pattern of Fig. 1(b) was received in two orientation variants. The same pattern, but observed as a superposition of diffractions from two orientation variants, was obtained in Ref. 11 and attributed to  $x \sim 0.1$ . Unfortunately, the pattern of Fig. 1(b) was overlooked in later publications. As we see, both patterns include the  $\{\frac{1}{2}\frac{1}{2}0\}$ -type spots but not the  $\{\frac{1}{2}00\}$ -type spots. The structures corresponding to these patterns have a  $\sqrt{2}a_0 \times 2\sqrt{2}a_0$  unit cell. The atomic structure related to the diffraction of Fig. 1(a) was suggested in Ref. 2.

Finally, Fig. 1(c) presents the most frequently observed pattern which was first found by Alario-Franco *et al.*<sup>9</sup> and later reported in many publications.<sup>7,10-12,14-16</sup> Besides the  $\{\frac{1}{4}\frac{1}{4}0\}$ -type spots, it also has the  $\{\frac{1}{2}00\}$ -type diffraction maxima, absent in Figs. 1(a) and 1(b). The pattern shown in Fig. 1(c) was attributed in Ref. 11 to the stoichiometry  $x \sim 0.85$ . The corresponding atomic structure has a  $2\sqrt{2}a_0 \times 2\sqrt{2}a_0$  unit cell.

The appearance of the  $\{\frac{1}{4}\frac{1}{4}0\}$  phases at small  $x$  (which is at odds with the existing theories of ordering) and also

the fact that, unlike the usual observed diffuse maxima of the O-II ordered phase, these phases give sharp and strong diffraction spots, sometimes resulted in the opinion<sup>3,14,15</sup> that these phases are not completely related to the oxygen ordering. However the recent quantitative neutron<sup>13,17</sup> and x-rays<sup>2</sup> single-crystal studies seem to dispel these doubts. In the majority of studies (exceptions are Refs. 11 and 18), the various  $\{\frac{1}{4}\frac{1}{4}0\}$  phases were all observed within the "tetragonal" region of stoichiometry, i.e., at small  $x < 0.4$ . The appearance of such a rich variety of different  $\{\frac{1}{4}\frac{1}{4}0\}$  phases within a narrow stoichiometry region requires an explanation. This also demonstrates that the issue of the oxygen ordering in this system is still far from being resolved. While part of the phase diagram at  $x > 0.5$ , describing the orthorhombic phases with the Cu-O [010] chain structures, is reasonably well studied, at least at moderate temperatures, this, however, cannot be said about the part at  $x < 0.4$ , related to the tetragonal nonsuperconducting region.

The purpose of this work is to address the problems related to the  $\{\frac{1}{4}\frac{1}{4}0\}$  phases and other oxygen-ordered structures formed in the  $\text{YBa}_2\text{Cu}_3\text{O}_{6+x}$  system at small  $x$ , i.e., in the "tetragonal" part of the phase diagram. The concentration-wave method<sup>19,20</sup> and the information about the superstructure wave vectors  $\mathbf{k}_j$ , contained in the diffraction patterns of Fig. 1, allow one to determine the sequence of oxygen-ordering phase transformations and the atomic structure of ordered phases at  $x < 0.4$ . The O-O interaction potential, consistent with the  $\{\frac{1}{4}\frac{1}{4}0\}$  structures in this stoichiometry region, is also estimated.

Using this potential as input data, we performed the computer simulation of the multiple oxygen ordering at  $x = 0.25$  which characterizes the atomic and mesoscopic structure rearrangements. Earlier, the same approach, the concentration-wave analysis combined with the analysis of diffraction data and the computer simulation of ordering, was employed to study the structure transformations in the superconducting  $\text{YBa}_2\text{Cu}_3\text{O}_{6+x}$  oxides at  $x > 0.4$ .<sup>1</sup>

## II. CONCENTRATION WAVE ANALYSIS OF THE $\{\frac{1}{4}\frac{1}{4}0\}$ PHASES FORMED AT SMALL $x$

The concentration-wave approach formulates the general symmetry constraints imposed on the atomic structure of stable ordered phases. These constraints give a guideline for analyzing a complicated picture of multiple ordering. The stable high-temperature ordered structures are known<sup>19,20</sup> to be the structures in most cases generated by the concentration waves whose wave vectors  $\{\mathbf{k}_j\}$  correspond to the Lifshitz points in the first Brillouin zone of a disordered phase.

The first Brillouin zone of the disordered tetragonal  $T$  phase in the  $\text{YBa}_2\text{Cu}_3\text{O}_{6+x}$  system has only three stars of the Lifshitz points,  $(000)$ ,  $\{\frac{1}{2}00\}$ , and  $(\frac{1}{2}\frac{1}{2}0)$ . These stars are responsible for the oxygen ordering in Cu(1)-(O) basal (001) planes in  $\text{YBa}_2\text{Cu}_3\text{O}_{6+x}$ . The  $(000)$  star generates the stable orthorhombic O-I phase, whereas the concentration wave  $\mathbf{k} = (2\pi/a_0)\{\frac{1}{2}00\}$  belonging to the  $\{\frac{1}{2}00\}$  star generates the double-period O-II ordered phase.<sup>1</sup>

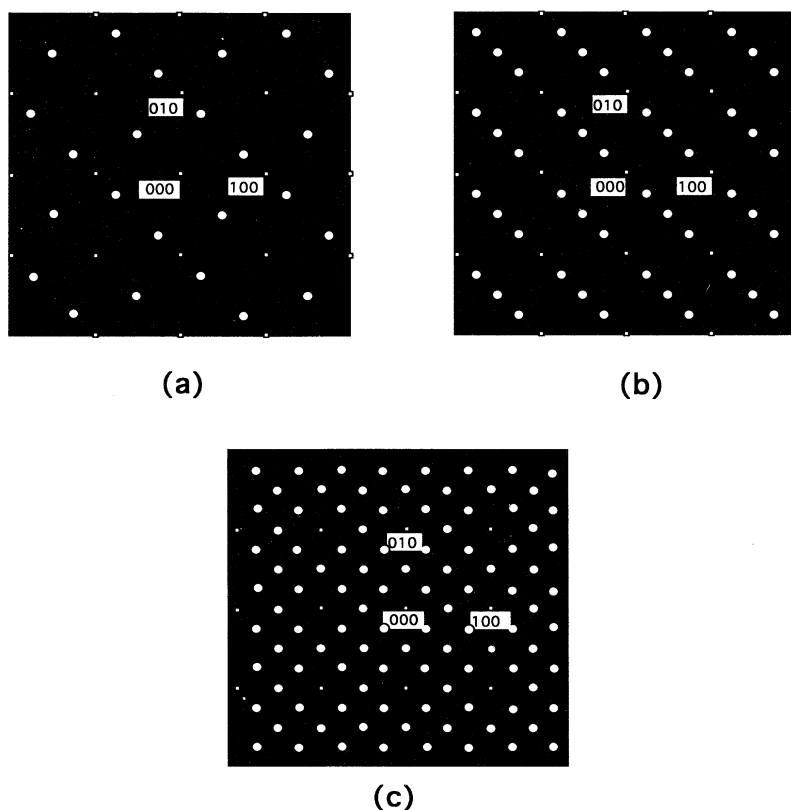


FIG. 1. Schematic presentation of three types of observed  $(HK0)$  diffraction patterns for the  $\{\frac{1}{4}\frac{1}{4}0\}$  phases in the  $\text{YBa}_2\text{Cu}_3\text{O}_{6+x}$  system: (a) x-ray diffraction from the  $\sqrt{2}a_0 \times 2\sqrt{2}a_0$  structure observed by Zeiske *et al.* (Ref. 2) from a single orientation variant of  $\text{YBa}_2\text{Cu}_3\text{O}_{6.35}$  ( $x = 0.35$ ); (b) the diffraction pattern of another  $\sqrt{2}a_0 \times 2\sqrt{2}a_0$  structure observed by Kemin *et al.*; (c) the most frequently observed diffraction for the  $2\sqrt{2}a_0 \times 2\sqrt{2}a_0$  structure (Refs. 7, 10–12, 14, 15, and others). The superstructure maxima are shown by large circles, the fundamental reflections by small points (indices of three fundamental reflections are marked).

Thus, the (000) and  $\{\frac{1}{2}00\}$  stars generate the most stable orthorhombic ordered phases, O-I and O-II, observed in this system. These phases are built as the Cu-O [010] chain structures. It will be shown below that the third Lifshitz star ( $\frac{1}{2}\frac{1}{2}0$ ) also plays an important role in generating the family of ordered phases in the  $\text{YBa}_2\text{Cu}_3\text{O}_{6+x}$  system at  $x < \sim 0.4$ , i.e., within a "tetragonal" region of stoichiometry.

#### A. Ordered structures related to the ( $\frac{1}{2}\frac{1}{2}0$ ) Lifshitz point

Diffraction patterns presented in Figs. 1(a) and 1(b), which are related to the  $\{\frac{1}{4}\frac{1}{4}0\}$  phases with  $\sqrt{2}a_0 \times 2\sqrt{2}a_0$  unit cell observed at  $x < \sim 0.4$ ,<sup>2,3</sup> do not contain the  $\{\frac{1}{2}00\}$ -type diffraction spots. Instead, they have the  $\{\frac{1}{2}\frac{1}{2}0\}$  diffraction spots. The latter is an indication that these phases are the superstructures of the primary ordered structure generated by the ( $\frac{1}{2}\frac{1}{2}0$ ) Lifshitz star.

To describe the positions of O atoms in an ordered structure, it is convenient to use the occupation probabilities  $n(p, \mathbf{r})$  to find an O atom in the interstitial site ( $p, \mathbf{r}$ ) where  $\mathbf{r}$  is the translation vector labeling the origin of a unit cell [the position of Cu(1) atom in our case] and the index  $p$  ( $p=1,2$ ) labels the type (or the sublattice) of interstitial site within this unit cell. The probability function  $n(p, \mathbf{r})$  can be always presented as a superposition of the concentration waves which are revealed on the diffraction pattern as the superlattice spots. The stability criteria I and II, found in Refs. 19 and 20 (see the Appendix), impose the very strong symmetry constraints on the amplitudes of the concentration waves which are able to generate a thermodynamically stable ordered phase. These constraints limit the number of possible ordered phases generated by the Lifshitz star ( $\frac{1}{2}\frac{1}{2}0$ ) to two:

$$n(p, \mathbf{r})_1 = \begin{cases} n(1, \mathbf{r})_1 = c + \eta_1 \exp(i\mathbf{k}_0 \cdot \mathbf{r}), \\ n(2, \mathbf{r})_1 = c + \eta_1 \exp(i\mathbf{k}_0 \cdot \mathbf{r}), \end{cases} \quad (1a)$$

and

$$n(p, \mathbf{r})_2 = \begin{cases} n(1, \mathbf{r})_2 = c + \eta_0 + (\eta_1 + \eta'_1) \exp(i\mathbf{k}_0 \cdot \mathbf{r}), \\ n(2, \mathbf{r})_2 = c - \eta_0 + (\eta_1 - \eta'_1) \exp(i\mathbf{k}_0 \cdot \mathbf{r}), \end{cases} \quad (1b)$$

where  $\mathbf{k}_0 = (2\pi/a_0)(\frac{1}{2}\frac{1}{2}0)$ ,  $\mathbf{r} = x_1\mathbf{a}_1 + x_2\mathbf{a}_2$ ,  $\mathbf{a}_1$  and  $\mathbf{a}_2$  are the perovskite lattice unit translations in (001) basal plane,  $x_1$  and  $x_2$  are the integer coordinates of the Bravais unit cells;  $\eta_1$  is the long-range-order (LRO) parameter related to the symmetric irreducible representation of the group of the wave vector  $\mathbf{k}_0$  whereas  $\eta_0$  and  $\eta'_1$  are the LRO parameters related to the antisymmetric irreducible representations of the groups of the wave vectors  $\mathbf{k} = \mathbf{0}$  and  $\mathbf{k}_0$ , respectively;  $c = N_O/2N$  is the overall oxygen stoichiometry [ $N_O$  is the total number of O atoms in the Cu(1)-O (001) basal plane, while  $N$  is the total number of the unit cells in this plane]. The constant terms  $c$ ,  $c + \eta_0$ , and  $c - \eta_0$  in Eqs. (1) actually give the fraction of interstitial sites in the corresponding sublattice,  $p=1$  or  $p=2$ , occupied by O atoms. Sum of them give the oxygen

stoichiometry  $x$ . It is always equal to  $2c$ , i.e.,  $x = 2c$ . As in all previous theories, we consider the two-dimensional (2D) model which is a good approximation to describe the ordering in the (001) basal plane.

$(\frac{1}{2}\frac{1}{2}0)_2$  phase. It follows from Eq. (1a) that the function  $n(p, \mathbf{r})_1$  describes the primary ordered structure where O atoms equally populate both interstitial sublattices ( $p=1,2$ ). This actually means that this structure is pseudotetragonal. In the completely ordered state the occupation probabilities  $n(p, \mathbf{r})$ , by definition, may assume only two values, either 1 or 0. Using this condition in Eq. (1a) gives the values  $c$  and  $\eta_1$  for the completely ordered (fully stoichiometric) primary ordered phase:  $c = \eta_1 = \frac{1}{2}$ . Placing O atoms in the sites where  $n(p, \mathbf{r})_1 = 1$  yields the structure shown in Fig. 2(a). Hereafter this phase is named  $(\frac{1}{2}\frac{1}{2}0)_2$  to reflect the star generating the ordered pattern and the equal occupation by O atoms of all two interstitial sublattices (subscript 2). Since O atoms occupy both interstitial sublattices, its diffraction pattern meets the extinction rules for some of the ( $\frac{1}{2}\frac{1}{2}0$ )-kind reflections in different Brillouin zones. The above-obtained value  $c = \frac{1}{2}$  corresponds to the stoichiometry  $x = 2c = 1$ . Therefore, in the relevant range  $x < 0.4$ , the  $(\frac{1}{2}\frac{1}{2}0)_2$  primary high-temperature ordered phase is strongly off-stoichiometric. To reach the stoichiometry  $x$  at low temperatures it should undergo a series of ordering reactions.

$(\frac{1}{2}\frac{1}{2}0)_1^{\text{centr}}$  phase. The ordered phase described by Eq. (1b) is generated by two stars, (000) and ( $\frac{1}{2}\frac{1}{2}0$ ). Different average occupations of two sublattices,  $c + \eta_0$  and  $c - \eta_0$ , make the first sublattice ( $p=1$ ) preferential. This results in the orthorhombic distortion proportional to the parameter  $\eta_0$ . The completely ordered state of this phase is achieved if  $c = \eta_0 = \eta_1 = \eta'_1 = \frac{1}{4}$ . Placing O atoms at the sites, where the function  $n(p, \mathbf{r})_2$  with these parameters assumes the value 1, gives the  $2a_0 \times 2a_0$  structure shown in Fig. 2(b). We designate it  $(\frac{1}{2}\frac{1}{2}0)_1^{\text{centr}}$  to reflect the star generating this structure, the fact of occupation of the only sublattice and the centered  $2a_0 \times 2a_0$  unit cell of this structure. The value  $c = \frac{1}{4}$  corresponds to the stoichiometry  $x = 2c = \frac{1}{2}$  which is also outside the range  $x < 0.4$ . Therefore, this phase is also off-stoichiometric and should also undergo the ordering to reach the stoichiometry  $x$ .

The function  $n(p, \mathbf{r})_2$  differs from  $n(p, \mathbf{r})_1$  by two additional LRO parameters,  $\eta_0$  and  $\eta'_1$ , appearing in Eq. (1b). Therefore, the  $(\frac{1}{2}\frac{1}{2}0)_1^{\text{centr}}$  phase described by  $n(p, \mathbf{r})_2$  is the superstructure of the  $(\frac{1}{2}\frac{1}{2}0)_2$  phase described by  $n(p, \mathbf{r})_1$ . Since two additional LRO parameters are involved, the  $(\frac{1}{2}\frac{1}{2}0)_2 \rightarrow (\frac{1}{2}\frac{1}{2}0)_1^{\text{centr}}$  ordering is the first-order transition.

As it has been mentioned above, the  $(\frac{1}{2}\frac{1}{2}0)_2$  and  $(\frac{1}{2}\frac{1}{2}0)_1^{\text{centr}}$  phases should undergo multiple ordering at low temperatures to adapt their stoichiometries to the current value of  $x$ . The presence of the superlattice maxima in the  $\{\frac{1}{4}\frac{1}{4}0\}$ -type positions in Figs. 1(a) and 1(b) indicate that this ordering involves the concentration-wave vectors  $\{\mathbf{k}_1\} = (2\pi/a_0)\{\frac{1}{4}\frac{1}{4}0\}$ . These concentration waves should be added to functions (1a) and (1b) so that the resultant function  $n(p, \mathbf{r})$  satisfies the constraints imposed

on the concentration-wave amplitudes by the stability criteria formulated in the Appendix. The corresponding procedure gives only two possible functions:

$$n(p, \mathbf{r})_1^{(2)} = \begin{cases} n(1, \mathbf{r})_1^{(2)} = c + \eta_1 \exp(i\mathbf{k}_0 \cdot \mathbf{r}) + 2\eta_2 \cos \mathbf{k}_1 \mathbf{r} , \\ n(2, \mathbf{r})_1^{(2)} = c + \eta_1 \exp(i\mathbf{k}_0 \cdot \mathbf{r}) - 2\eta_2 \cos \mathbf{k}_1 \mathbf{r} , \end{cases} \quad (2a)$$

and

$$n(p, \mathbf{r})_2^{(2)} = \begin{cases} n(1, \mathbf{r})_2^{(2)} = c + \eta_0 + (\eta_1 + \eta'_1) \exp(i\mathbf{k}_0 \cdot \mathbf{r}) + 2(\eta_2 + \eta'_2) \cos \mathbf{k}_1 \mathbf{r} , \\ n(2, \mathbf{r})_2^{(2)} = c - \eta_0 + (\eta_1 - \eta'_1) \exp(i\mathbf{k}_0 \cdot \mathbf{r}) + 2(\eta_2 - \eta'_2) \cos \mathbf{k}_1 \mathbf{r} . \end{cases} \quad (2b)$$

Equations (2) describe the ordered  $\{\frac{1}{4}\frac{1}{4}0\}$  phases. In Eq. (2b),  $\eta_2$  and  $\eta'_2$  are the LRO parameters related to the symmetric and antisymmetric irreducible representations of the group of the wave vector  $\mathbf{k}_1$ , respectively.

$(\frac{1}{4}\frac{1}{4}0)_2$  phase. The function  $n(p, \mathbf{r})_1^{(2)}$  describes the secondary structure with the same occupation of both sublattices. Thus, this structure is pseudotetragonal. It is designated below as the  $(\frac{1}{4}\frac{1}{4}0)_2$  phase where the subscript 2 indicates that both interstitial sublattices are equally occupied. The completely ordered state of this secondary ordered  $(\frac{1}{4}\frac{1}{4}0)_2$  phase is attained if  $c = \eta_1 = \eta_2 = \frac{1}{4}$ . The structure of this phase is shown in Fig. 2(c). The  $(\frac{1}{4}\frac{1}{4}0)_2$  phase is the superstructure of the primary ordered phase  $(\frac{1}{2}\frac{1}{2}0)_2$ . The value  $c = \frac{1}{4}$ , obtained above, corresponds to the stoichiometry  $x = 2c = 0.5$ .

Therefore, this phase is still off-stoichiometric in the range  $x < 0.4$  [for a sample studied in Refs. 2 and 13 with  $x = 0.35$ , the maximum occupation probability given by  $n(p, \mathbf{r})_1^{(2)}$  is  $4c = 2x = 0.7$  rather than 1]. Since O atoms occupy both interstitial sublattices, its diffraction pattern meets the extinction rules for some of the  $\{\frac{1}{4}\frac{1}{4}0\}$  and  $\{\frac{1}{2}\frac{1}{2}0\}$  kinds of reflections in different Brillouin zones. The diffraction pattern generated by the  $(\frac{1}{4}\frac{1}{4}0)_2$  structure is the same as the one presented in Fig. 1(a). With the accuracy of atomic displacements, the  $(\frac{1}{4}\frac{1}{4}0)_2$  structure [Fig. 2(c)] coincides with the structure obtained by Zeiske *et al.*<sup>2</sup> from the x-ray single-crystal diffraction data. It should be specially emphasized that the pseudotetragonal character of the  $(\frac{1}{2}\frac{1}{2}0)_2$  and  $(\frac{1}{4}\frac{1}{4}0)_2$  phases should drastically change the strain-accommodating morphology

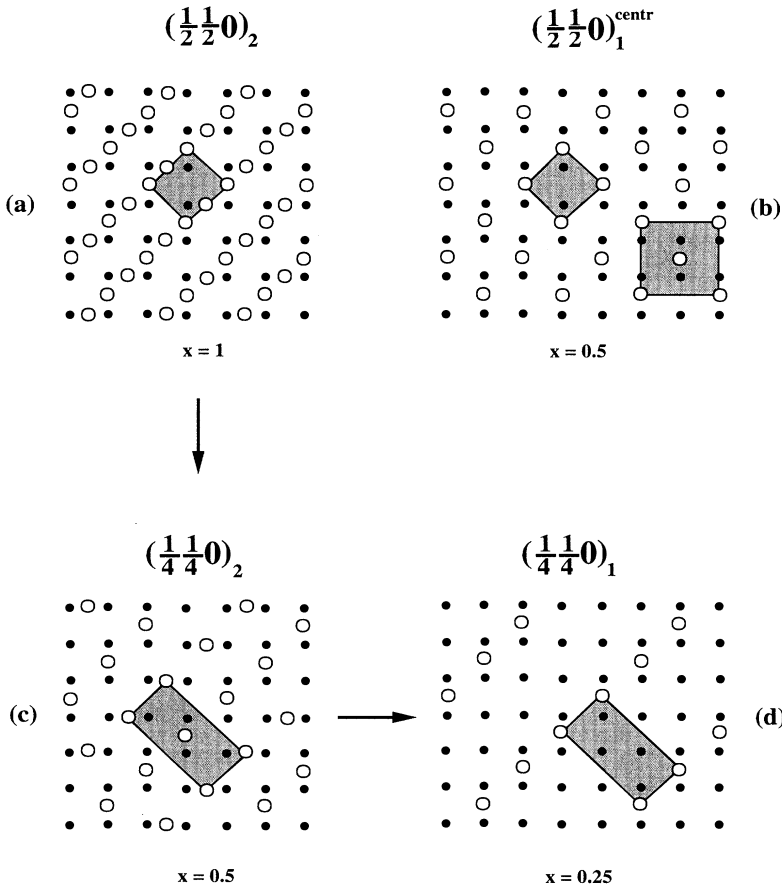


FIG. 2. The [110] oxygen chain superstructures (a)–(d) at  $x < \sim 0.35$ , generated by the  $(\frac{1}{2}\frac{1}{2}0)$  Lifshitz star. The structures are described by Eqs. (1a), (1b), (2a), and (2b), respectively. The  $(\frac{1}{4}\frac{1}{4}0)_2$  (c) and  $(\frac{1}{4}\frac{1}{4}0)_1$  (d) are the secondary and tertiary ordered structures with a  $\sqrt{2}a_0 \times 2\sqrt{2}a_0$  unit cell. Their diffraction patterns are shown in Figs. 1(a) and 1(b). The transitions order [sequence (3) or (22c)] upon cooling is shown by arrows.

(with respect to the morphology of orthorhombic phases). The (110) transformation twins, accommodating the elastic strain caused by the tetragonal→orthorhombic crystal lattice distortion, should not be formed in these cases.

The atomic structure described by the function  $n(p, r)_1^{(2)}$  has been suggested in the phenomenological short chain ordering model<sup>21</sup> for the stoichiometry  $x=0.5$ . It can be also found in the list of possible ground-state structures suggested by Aligia *et al.*<sup>22</sup>

$(\frac{1}{4}\frac{1}{4}0)_1$  phase. The second function  $n(p, r)_2^{(2)}$ , given by Eq. (2b), describes the completely ordered structure if

$$c = \eta_0 = \eta_1 = \eta'_1 = \eta_2 = \eta'_2 = \frac{1}{8}.$$

Then it gives the structure shown in Fig. 2(d). The value  $c = \frac{1}{8}$  corresponds to the stoichiometry  $x = 2c = 0.25$  which is within the range  $x < 0.4$ . Therefore, this phase does not undergo the further ordering transformation in this composition range. For this structure, the average occupation numbers in two sublattices,  $c + \eta_0$  and  $c - \eta_0$ , are different. The first sublattice with a higher occupation is preferential. Because of that, this structure is orthorhombic and thus should form the (110) accommodation twins. We designate this phase as the  $(\frac{1}{4}\frac{1}{4}0)_1$  phase where the subscript 1 indicates that one interstitial sublattice is preferentially occupied. Comparing Eqs. (2a) and (2b) shows that the  $(\frac{1}{4}\frac{1}{4}0)_1$  phase, whose ideal stoichiometry is  $x = 0.25$ , is the superstructure of the  $(\frac{1}{4}\frac{1}{4}0)_2$  phase.

Since the ideal stoichiometry  $x = 0.5$  of the secondary ordered pseudotetragonal  $(\frac{1}{4}\frac{1}{4}0)_2$  phase is outside the relevant range  $x < 0.4$ , the tertiary ordering  $(\frac{1}{4}\frac{1}{4}0)_2 \rightarrow (\frac{1}{4}\frac{1}{4}0)_1$  brings the stoichiometry inside this range. Thus it should be expected at low temperatures. Because this ordering is the first-order transition, it develops through the nucleation mechanism. The  $(\frac{1}{4}\frac{1}{4}0)_1$  phase [Fig. 2(d)] generates the diffraction pattern which coincides with that shown in Fig. 1(b). It was observed in two orientation variants by Kemin *et al.*<sup>3</sup> and as a superposition of two orientation variants, by Alario-Franco *et al.*<sup>11</sup> (the stoichiometry of the sample was attributed to  $x \sim 0.1$ ). Comparison of the diffraction patterns of Figs. 1(a) and 1(b) (observed in Refs. 2 and 3), related to  $(\frac{1}{4}\frac{1}{4}0)_2$  and the  $(\frac{1}{4}\frac{1}{4}0)_1$  structures, respectively, indicates that both structures have the same  $\sqrt{2}a_0 \times 2\sqrt{2}a_0$  unit cell. The difference between them is the absence of certain  $\{\frac{1}{2}\frac{1}{2}0\}$  and  $\{\frac{1}{4}\frac{1}{4}0\}$  kinds of reflections on the pattern of Fig. 1(a) related to the  $(\frac{1}{4}\frac{1}{4}0)_2$  phase. These extinction rules are eliminated when the  $(\frac{1}{4}\frac{1}{4}0)_2 \rightarrow (\frac{1}{4}\frac{1}{4}0)_1$  tertiary ordering, resulting in the transition of O atoms from one of the O sublattices into another, occurs.

Figure 2 shows all atomic structures generated by the  $(\frac{1}{2}\frac{1}{2}0)$  Lifshitz star which are the superstructures of the  $(\frac{1}{2}\frac{1}{2}0)_2$  phase. All of them, including the latter, are the [110] chain structures formed by alternating oxygen-atom chains along the [110] direction.

### B. Sequence of ordering transformations

It follows from foregoing that at  $x < 0.4$  the expected sequence of ordering transformations in  $\text{YBa}_2\text{Cu}_3\text{O}_{6+x}$

upon cooling, which is consistent with the observed diffraction patterns of Figs. 1(a) and 1(b), is

$$T \rightarrow (\frac{1}{2}\frac{1}{2}0)_2 \rightarrow (\frac{1}{4}\frac{1}{4}0)_2 \rightarrow (\frac{1}{4}\frac{1}{4}0)_1. \quad (3)$$

Although the alternative sequences  $T \rightarrow (\frac{1}{2}\frac{1}{2}0)_2 \rightarrow (\frac{1}{4}\frac{1}{4}0)_1$  or

$$T \rightarrow (\frac{1}{2}\frac{1}{2}0)_2 \rightarrow (\frac{1}{2}\frac{1}{2}0)_1^{\text{centr}} \rightarrow (\frac{1}{4}\frac{1}{4}0)_1$$

could be, in principle, expected, they however should be ruled out because they do not include the  $(\frac{1}{4}\frac{1}{4}0)_2$  phase whose diffraction pattern [Fig. 1(a)] was observed in Refs. 2 and 3.

Sequence (3) includes two pseudotetragonal phases,  $(\frac{1}{2}\frac{1}{2}0)_2$  and  $(\frac{1}{4}\frac{1}{4}0)_2$ , formed at higher temperatures, and the low-temperature orthorhombic  $(\frac{1}{4}\frac{1}{4}0)_1$  phase. Only the latter forms the (110) elastic-strain accommodating twins. Therefore, when the transformation sequence (3) is observed in the opposite direction, upon heating, it should result in the orthorhombic→pseudotetragonal transition  $(\frac{1}{4}\frac{1}{4}0)_1 \rightarrow (\frac{1}{4}\frac{1}{4}0)_2$  and thus in disappearance of the (110) twin morphology. This prediction, following from the concentration-wave analysis, seems to be confirmed by Kemin *et al.*,<sup>3</sup> who observed dense (110) microtwins of the orthorhombic  $\{\frac{1}{4}\frac{1}{4}0\}$  phase at more low temperatures and the orthorhombic→tetragonal transition (disappearance of microtwins) upon heating, the  $\{\frac{1}{4}\frac{1}{4}0\}$ -type superstructure maxima being present in both phases, orthorhombic and tetragonal (pseudotetragonal).

It is important that the ordering sequence (3) realized at  $x < 0.4$  radically differs from the sequence

$$T \rightarrow \text{O-I} \rightarrow \text{O-II} \quad (4)$$

observed upon cooling the tetragonal  $T$  phase in the other stoichiometry range,  $x > 0.4-0.5$ . It will be shown in Sec. III A that the cooling of the O-II phase in this stoichiometry range may result in appearance of the  $\{\frac{1}{4}\frac{1}{4}0\}$  phases. These phases are formed from the O-II secondary ordered phase by the tertiary ordering transition  $\text{O-II} \rightarrow \{\frac{1}{4}\frac{1}{4}0\}$ . Being the superstructures of the O-II phase, they inherit its  $\{\frac{1}{2}00\}$ -type diffraction spots. These phases, which are the superstructures of the O-II phase, are different from the  $\{\frac{1}{4}\frac{1}{4}0\}$  phases formed at  $x < 0.4$ . The latter are the superstructures of the  $(\frac{1}{2}\frac{1}{2}0)_2$  phase and thus do not have the  $\{\frac{1}{2}00\}$ -type diffraction spots.

### III. RELATION BETWEEN ORDERED STRUCTURES AND O-O INTERACTION POTENTIALS

In terms of the pairwise O-O interaction model, the stability of different ordered structures is determined by the minima of eigenvalues of the Fourier transform  $V(\mathbf{k})_{pq}$  of the O-O pairwise interaction potentials  $W(\mathbf{r}-\mathbf{r}')_{pq}$ :

$$V(\mathbf{k})_{pq} = \sum_{\mathbf{r}} W(\mathbf{r})_{pq} \exp(-i\mathbf{k}\cdot\mathbf{r}), \quad (5)$$

where  $(p, \mathbf{r})$  and  $(q, \mathbf{r}')$  are the coordinates of interacting

O atoms;  $p, q = 1, 2$ . The spectrum of eigenvalues of the  $2 \times 2$  matrix of  $V(\mathbf{k})_{pq}$  forms two branches,  $\lambda(\mathbf{k})_+$  and  $\lambda(\mathbf{k})_-$ , where  $\lambda(\mathbf{k})_+ > \lambda(\mathbf{k})_-$ . The values  $\lambda(\mathbf{k})_+$  and  $\lambda(\mathbf{k})_-$  are the eigenvalues corresponding to the symmetric and antisymmetric representations of the group of the vector  $\mathbf{k}$ . The symmetry of the primary ordered phase is determined by the eigenfunctions  $v(p, \mathbf{k}_0)_- \times \exp(i\mathbf{k}_0\mathbf{r})$  related to the eigenvalue  $\lambda(\mathbf{k}_0)_-$  which provides the global minimum of  $\lambda(\mathbf{k})_-$ .<sup>19,20</sup>

Since the trace of the matrix  $W(\mathbf{r}-\mathbf{r}')_{pq}$  is an invariant and the occupation of the same site by two O atoms is forbidden [i.e.,  $W(0)_{pp} = 0$ ], we have

$$\text{Tr}[W(\mathbf{r}-\mathbf{r}')_{pq}] = \sum_{\mathbf{k}} [\lambda(\mathbf{k})_+ + \lambda(\mathbf{k})_-] = 0.$$

The latter identity implies that the eigenvalues  $\lambda(\mathbf{k})_+$  and  $\lambda(\mathbf{k})_-$  assume both negative and positive values at different  $\mathbf{k}$ , and thus the global minimum of  $\lambda(\mathbf{k})_-$  is always negative [ $\lambda(\mathbf{k}_0)_- < 0$ ].

It should be mentioned that, by definition, the spectrum  $\lambda(\mathbf{k})_-$  has extrema at all of the Lifshitz points, irrespective of the choice of the potential  $W(\mathbf{r}-\mathbf{r}')_{pq}$ . A specific choice of the potential just determines the values of the extrema at the Lifshitz points and the kind of these extrema (minimum, maximum, or saddle point). The values of  $\lambda(\mathbf{k})_-$  at the Lifshitz points usually determine the main features of the topology of the  $\lambda_- = \lambda(\mathbf{k})_-$  surface in the first Brillouin zone of a disordered phase, which, in turn, determine the structures and ordering transformation sequence upon the cooling of a disordered phase. Particularly, the primary ordering provides the first step in the transition sequence (3), viz., the  $T \rightarrow (\frac{1}{2}\frac{1}{2}0)_2$  transition, at  $x < 0.4$ , if the interaction potential  $W(\mathbf{r})_{pq}$  is such that the global minimum of the function  $\lambda(\mathbf{k})_-$  is at the Lifshitz point  $\mathbf{k} = \mathbf{k}_0 = (2\pi/a_0)(\frac{1}{2}\frac{1}{2}0)$ . On the other hand, at  $x > 0.4$ , where the primary ordering results in the  $T \rightarrow \text{O-I}$  transition [sequence (4)], the potential  $W(\mathbf{r})_{pq}$  should provide the global minimum of  $\lambda(\mathbf{k})_-$  at  $\mathbf{k} = 0$  [its eigenvector  $v(p, 0)_- = [v(1, 0)_-, v(2, 0)_-] = (1/\sqrt{2})(1, \bar{1})$  describes the homogeneous transition of O atoms from the second to the first interstitial sublattice].

Therefore, the  $T \rightarrow (\frac{1}{2}\frac{1}{2}0)_2$  primary ordering [sequence (3)] occurs at  $x < 0.4$  if

$$\lambda(\frac{1}{2}\frac{1}{2}0)_- = \min[\lambda(\mathbf{k})_-] < \lambda(000)_-, \quad (6a)$$

within this range, whereas the  $T \rightarrow \text{O-I}$  primary ordering [sequence (4)] occurs at  $x > 0.4$  if within this range

$$\lambda(000)_- = \min[\lambda(\mathbf{k})_-] < \lambda(\frac{1}{2}\frac{1}{2}0)_-. \quad (6b)$$

Comparison of (6a) and (6b) indicates that the spectrum  $\lambda(\mathbf{k})_-$  should depend on the oxygen concentration  $x$  so that it changes the relation between  $\lambda(000)_-$  and  $\lambda(\frac{1}{2}\frac{1}{2}0)_-$  with the concentration. To provide the ordering sequence (3) below  $x \sim 0.4$  and the sequence (4) above  $x \sim 0.4$ , the O-O pairwise interaction potentials  $W(\mathbf{r}-\mathbf{r}')_{pq}$  should change around  $x \sim 0.4$ . This change of the potential is not unexpected. Near the same stoichiometry  $x \sim 0.4$  (within  $\sim 0.35 < x < \sim 0.45$ ), many

important materials properties of  $\text{YBa}_2\text{Cu}_3\text{O}_{6+x}$ , such as the lattice parameters, different types of bondlengths, bond valence sums, etc., also drastically change.<sup>18,23</sup> The electronic spectrum in this range undergoes a major reconstruction as well, resulting in a loss of superconductivity and transition from a metal to a semiconductor state.

Below in this section, the estimates of the  $\lambda(\mathbf{k})_-$  for three Lifshitz stars (000),  $\{\frac{1}{2}00\}$ , and  $(\frac{1}{2}\frac{1}{2}0)$  at different  $x$  are presented. They show that the O-O potential should drastically change between  $x \sim 0.25-0.3$  and  $0.40-0.45$  to provide the agreement with observed structure transformations. The other important result following from these estimates is the appearance of the third type of transformation sequence within a small intermediate region of  $x$ , this sequence being different from both the (3) and (4) ones.

Since there is no sufficient information about the width and location of this small intermediate region, we assume it to be within the interval  $\sim 0.35 < x < \sim 0.4$ . This assumption is based on the following: (i) according to Ref. 2, the  $(\frac{1}{4}\frac{1}{4}0)_2$  phase, realized in sequence (3), forms at  $x \sim 0.35$ , (ii) according to Ref. 24, the orthorhombic O-II phase, realized in sequence (4), forms at  $x \sim 0.4$ . This estimate of the intermediate region, between  $x \sim 0.35$  and  $0.4$ , agrees with the findings<sup>23</sup> that the orthorhombic  $\rightarrow$  tetragonal and superconductor  $\rightarrow$  semiconductor transitions occur between  $x = 0.34$  and  $0.38$ . Hereafter we consider three physically different regions of oxygen stoichiometry:  $x < \sim 0.35$ ,  $x > \sim 0.4$ , and the small intermediate region  $\sim 0.35 < x < \sim 0.4$ .

#### A. Range $x > 0.4$

Condition (6b) characterizing this range is, in fact, the condition of the  $T \rightarrow \text{O-I}$  primary ordering. Another condition, which is necessary to observe also the  $\text{O-I} \rightarrow \text{O-II}$  secondary transition within this concentration range, is

$$\lambda(\frac{1}{2}00)_- < \lambda(\frac{1}{2}\frac{1}{2}0)_- \quad (7)$$

[otherwise, if  $\lambda(\frac{1}{2}\frac{1}{2}0)_- < \lambda(\frac{1}{2}00)_-$ , then the  $\text{O-I} \rightarrow (\frac{1}{2}\frac{1}{2}0)_1^{\text{centr}}$  secondary ordering rather than the  $\text{O-I} \rightarrow \text{O-II}$  ordering would occur]. Therefore, combining (6b) and (7), we arrive at the conclusion that the necessary condition to obtain the observed ordering sequence  $T \rightarrow \text{O-I} \rightarrow \text{O-II}$  [Eq. (4)] within the relevant range,  $x > 0.4$ , requires the interaction potentials to meet the chain of inequalities:

$$\lambda(000)_- < \lambda(\frac{1}{2}00)_- < \lambda(\frac{1}{2}\frac{1}{2}0)_-. \quad (8)$$

At low temperatures and  $x > 0.5$ , according to different studies, the off-stoichiometric O-II phase adapts its structure in different ways: the excess O atoms are incorporated either into the interstitial plane faults in the O-II structure forming the Magneli-type phases<sup>4-8,25</sup> or by formation of a "glassy" (short-range order) state consisting of the antiphase nanoscale domains of the O-II structure whose domain boundary absorbs the excessive O atoms (or excessive oxygen vacancies).<sup>1</sup> In the last case,

the size of the domains should depend on  $x$ , decreasing with deviation from  $x=0.5$ . Experimentally, this effect was observed in Refs. 18, 26, and 27. It follows from the bulk neutron-diffraction data<sup>26</sup> that the O-II phase is observed only in the form of this "glassy" (short-range order) state at all compositions. The exception is the case of the nearly exact O-II phase stoichiometry  $x=0.5$ , at which the domains become macroscopically large (besides, a special condition of a very slow cooling, is required<sup>6,7,1</sup>) and thus give the sharp superlattice spots on the diffraction patterns.

However, if the function  $V(\mathbf{k})$

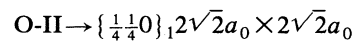
$$V(\mathbf{k}) = \frac{V(\mathbf{k})_{22} + V(\mathbf{k} - \mathbf{k}_{1/2\ 00})_{22}}{2} \quad (9)$$

has its minimum at the  $\{\frac{1}{4}\frac{1}{4}0\}$  point, then another phenomena has to occur at low temperatures.<sup>20</sup> This is the tertiary ordering O-II  $\rightarrow \{\frac{1}{4}\frac{1}{4}0\}_1$  producing the  $\{\frac{1}{4}\frac{1}{4}0\}_1$  phase with the  $2\sqrt{2}a_0 \times 2\sqrt{2}a_0$  unit cell (only one of the O sublattices is occupied in the completely ordered state). Its diffraction pattern is similar to that shown in Fig. 1(c): besides the  $\{\frac{1}{4}\frac{1}{4}0\}$ -type maxima, it has the  $\{\frac{1}{2}00\}$ -type diffraction maxima inherited from the parent O-II phase. This  $\{\frac{1}{4}\frac{1}{4}0\}_1$  phase becomes then the most stable phase at

low temperatures.

It is interesting that the O-O potential, estimated at  $x=0.5$  in previous studies<sup>1,28,29</sup> (it includes the anisotropic screened-Coulomb potential, the strain-induced interaction potential, and the short-range correction  $\delta W_1$ ), indeed, provides the minimum of the function  $V(\mathbf{k})$  in (9) at the points  $\{\mathbf{k}_1\} = (2\pi/a_0)\{\frac{1}{4}\frac{1}{4}0\}$ . Therefore, the  $\{\frac{1}{4}\frac{1}{4}0\}_1$  phase with a  $2\sqrt{2}a_0 \times 2\sqrt{2}a_0$  unit cell should form at low temperatures as a stable tertiary phase. It forms in the tertiary ordering transition O-II  $\rightarrow \{\frac{1}{4}\frac{1}{4}0\}_1$  which, according to the computer simulations,<sup>1,29</sup> results in formation of, at least, two low-temperature  $2\sqrt{2}a_0 \times 2\sqrt{2}a_0$  phases for relevant composition range. These phases, having the stoichiometries  $x = \frac{3}{4}$  and  $x = \frac{5}{8}$ , are named below as  $\alpha - \{\frac{1}{4}\frac{1}{4}0\}_1$  and  $\beta - \{\frac{1}{4}\frac{1}{4}0\}_1$ , respectively. Their structures and the corresponding diffraction patterns are shown in Figs. 3(c) and 3(d).

Since the



transition is of the first order, it occurs at low temperatures through the nucleation mechanism and, thus, is kinematically hindered. But these  $\{\frac{1}{4}\frac{1}{4}0\}_1$  phases may still form at (110) twin boundaries playing a role of nu-

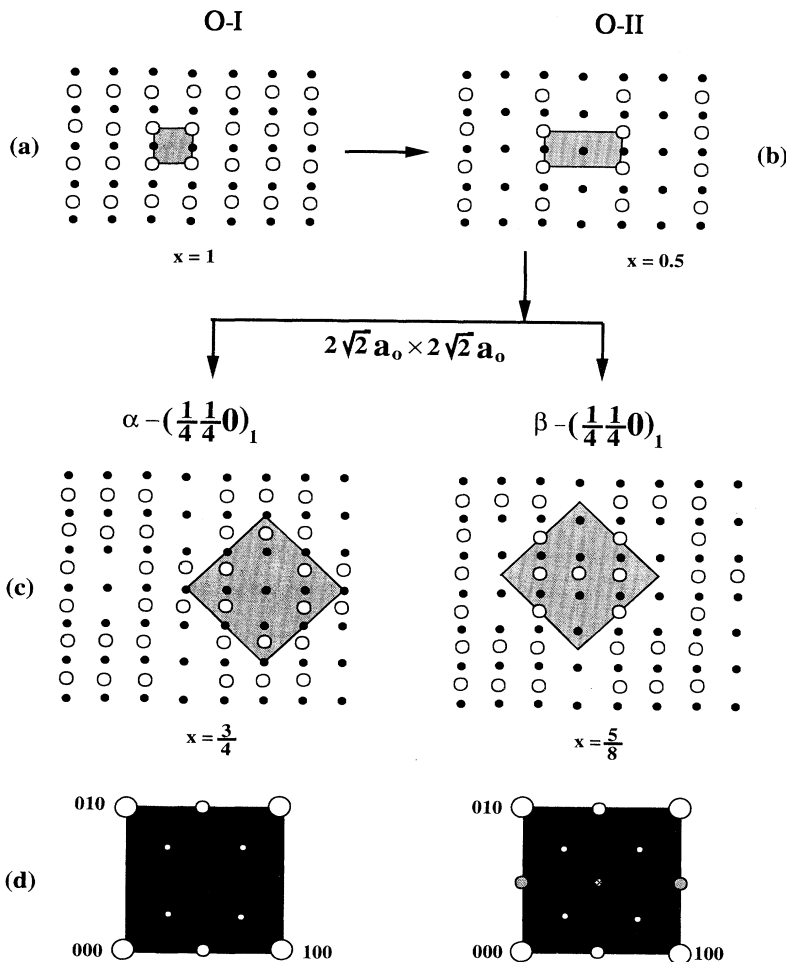


FIG. 3. The [010] Cu-O chain superstructures (with corresponding stoichiometries  $x$ ) generated by the (000) Lifshitz star at  $x \sim 0.4-0.45$ . The observed O-I and double-period O-II ordered structures correspond to the Lifshitz points (000) and  $\{\frac{1}{2}00\}$ . The  $\alpha - (\frac{1}{4}\frac{1}{4}0)_1$  and  $\beta - (\frac{1}{4}\frac{1}{4}0)_1$  phases (c) with a  $2\sqrt{2}a_0 \times 2\sqrt{2}a_0$  unit cell are the tertiary ordered superstructures of the secondary ordered O-II phase. Their diffraction patterns are shown in (d). The transitions order [sequence (4) or (22a)] upon cooling is shown by arrows.

creation sites.<sup>1,29</sup> They were observed in Refs. 11 and 18 [for the compositions  $x \sim 0.85$  (Ref. 11) and  $x \sim 0.64$  (Ref. 18)].

### B. Range $x < \sim 0.35$

In this range [where the transformation sequence (3) holds], the following estimate of the O-O interaction potential  $W(\mathbf{r})_{pq}$  can be made. It was shown above that to ensure the primary  $T \rightarrow (\frac{1}{2}\frac{1}{2}0)_2$  ordering at  $x < 0.35$ , the minimum of  $\lambda(\mathbf{k})_-$  must be at the  $(\frac{1}{2}\frac{1}{2}0)$  point [Eq. (6a)]. Then the entire transformation sequence [Eq. (3)] turns out to be completely different from the one [sequence (4)] occurring at  $x > 0.4$  [the sequence (4) realizes if the minimum of  $\lambda(\mathbf{k})_-$  falls at the (000) point] [Eq. (6b)].

Besides, the ordering sequence (3) realizes if the formation of the above-discussed  $2\sqrt{2}a_0 \times 2\sqrt{2}a_0$  structure (formed from the O-II phase) is avoided and, instead, the  $(\frac{1}{4}\frac{1}{4}0)_2$  phase with the  $\sqrt{2}a_0 \times \sqrt{2}a_0$  unit cell is formed. To avoid the formation of the O-II phase, which is a precursor of the  $\alpha$ - and  $\beta$ - $\{\frac{1}{4}\frac{1}{4}0\}_1$  phases, the relation

$$\lambda(\frac{1}{2}\frac{1}{2}0)_- < \lambda(000)_- < \lambda(\frac{1}{2}00)_- \quad (10)$$

should hold, where  $\lambda(\frac{1}{2}00)_-$  becomes the largest eigenvalue. As we see, these relations (10) providing sequence (3) are completely different from relations (8) which are necessary to ensure the sequence (4) at  $x > 0.4$ .

$$W(\mathbf{r}-\mathbf{r}')_{pq}^f = \begin{cases} \frac{(z^*)^2}{a_i} \exp\left[-\frac{a_i}{r_D}\right] + \delta W_i & \text{for } i \neq 2 \text{ at } |\mathbf{r}-\mathbf{r}'| \neq a_0, \\ (1 \pm f) \frac{(z^*)^2}{a_0} \exp\left[-\frac{a_0}{r_D}\right] + \delta W_2 & \text{for } i = 2 \text{ at } |\mathbf{r}-\mathbf{r}'| = a_0. \end{cases} \quad (13)$$

Here  $a_i$  are the radii of O-O coordination shells numbered by the integer  $i$  in order of their increase characterizing different distances between interstitial sites ( $p, \mathbf{r}$ ) and ( $q, \mathbf{r}'$ ),  $a_0$  is the perovskite lattice parameter,  $z^*$  is the effective oxygen charge including the dielectric constant,  $r_D$  is the screening radius,  $f$  is the anisotropy factor for the next-nearest intersite distance ( $i=2$ ) which is used with the sign  $(-)$  for the O-O interaction across a Cu atom and with the sign  $(+)$  otherwise;  $\delta W_i$  are the deviations from the screened Coulomb asymptotic associated with the spatial dispersion of the dielectric constant for the interaction of O atoms in near interstitial sites.

In the previous analysis,<sup>1,28,29</sup> a more simple potential  $W(\mathbf{r}-\mathbf{r}')_{pq}^f$  adjusted to obtain the experimentally observed transition temperatures at  $x=0.5$  was used. It contained only the deviation  $\delta W_1$  and the anisotropy factor  $f=0.5$  (it is similar to the anisotropic screened Coulomb potential used by Aligia *et al.*<sup>30</sup>). However, the potential  $W(\mathbf{r}-\mathbf{r}')_{pq}^f$  valid for the relevant interval  $x < 0.35$  cannot be mapped in such a simple model. To be consistent with observation results, a more general form (13), which includes the deviations  $\delta W_i$  in several coordination spheres, have to be used. It was also found

To estimate the value  $\lambda(\frac{1}{2}\frac{1}{2}0)_-$  in (10), we can compare the calculated mean-field transition temperature  $T_0$  for the  $T \rightarrow (\frac{1}{2}\frac{1}{2}0)_2$  transition, given by the equation

$$T_0 = -c(1-c) \frac{\lambda(\frac{1}{2}\frac{1}{2}0)_-}{k_B} \quad (11a)$$

(where  $k_B$  is the Boltzmann constant) with the observed transformation temperature. According to Ref. 15, the superstructure reflections of  $\{\frac{1}{4}\frac{1}{4}0\}$  phases disappear upon heating inside the electron microscope at about  $\sim 550$ – $570^\circ\text{C}$ . In a similar experiment<sup>14</sup> for a sample with  $x=0.25$ , the  $\{\frac{1}{4}\frac{1}{4}0\}$  phase was found to form at  $T > 500^\circ\text{C}$ . We use these data to estimate the temperature  $T_0$  in (11a). Assuming  $T_0 \sim 830$  K ( $560^\circ\text{C}$ ) at  $x=0.25$  ( $c=0.125$ ), we have, from Eq. (11a),

$$\lambda(\frac{1}{2}\frac{1}{2}0)_- \sim -(7610 \text{ K})k_B. \quad (11b)$$

This value was used to find the O-O potential for  $x < \sim 0.35$ . In this work we used the same class of the O-O potential that was used previously.<sup>1,28,29</sup> As before, it was assumed to consist of two parts: the anisotropic screened-Coulomb potential  $W(\mathbf{r}-\mathbf{r}')_{pq}^f$  and the strain-induced interaction potential  $W(\mathbf{r}-\mathbf{r}')_{pq}^{\text{elast}}$ :

$$W(\mathbf{r}-\mathbf{r}')_{pq} = W(\mathbf{r}-\mathbf{r}')_{pq}^f + W(\mathbf{r}-\mathbf{r}')_{pq}^{\text{elast}}, \quad (12)$$

where  $W(\mathbf{r}-\mathbf{r}')_{pq}^f$  has the form

that the relations (10) between the eigenvalues  $\lambda(\mathbf{k})_-$ , related to the Lifshitz points  $(\frac{1}{2}\frac{1}{2}0)$ , (000), and  $\{\frac{1}{2}00\}$ , are not sufficient to provide the transformation sequence (3) at  $x < 0.35$ . The other constraints have to be met also. Particularly, the specific numerical ratios between these three eigenvalues are required in relation (10). This imposes a very strong limitation on a possible form of the O-O potential (13).

Using the above found value  $\lambda(\frac{1}{2}\frac{1}{2}0)_- = -7610^\circ k_B$ , we tested in our computer simulations a large variety of different parameters in the electrostatic part of the O-O potential given by Eq. (13) to find the best fit to the available experimental data.<sup>2,3</sup> An interesting result following from this analysis is that the secondary ordering invariably produces the  $(\frac{1}{2}\frac{1}{2}0)_2 \rightarrow (\frac{1}{4}\frac{1}{4}0)_2$  transition, generated by the vector  $\mathbf{k}_1 = (2\pi/a_0)(\frac{1}{4}\frac{1}{4}0)$ . This result is practically insensitive to the choice of interaction parameters as long as condition (10) holds. On the other hand, the  $(\frac{1}{4}\frac{1}{4}0)_2 \rightarrow (\frac{1}{4}\frac{1}{4}0)_1$  transformation, involving the star (000), turns out to be very sensitive to the choice of interaction parameters. A wrong choice results in formation of a stable "glassy" state consisting of ultrafine mixture of

domains of  $(\frac{1}{4}\frac{1}{4}0)_2$  and  $(\frac{1}{4}\frac{1}{4}0)_1$  phases. This state produces the short-range diffuse maxima rather than the sharp superlattice spots that are really observed in Refs. 2 and 3 [Figs. 1(a) and 1(b)].

The best potential, providing the smallest (and simultaneously the shortest-range) deviations  $\delta W_i$ , gives the following parameters in (13):

$$\begin{aligned} r_D &\approx 4a_0/\sqrt{2}, \\ \delta W_1 &= -392^\circ k_B, \\ \delta W_2 &= 441^\circ k_B, \\ \delta W_3 &= -415^\circ k_B, \\ \delta W_4 &= -105^\circ k_B, \\ \delta W_5 &= 133^\circ k_B, \\ \delta W_i &= 0 \text{ at } i > 5, \\ f &\sim 0.07, \\ z^* &= 0.287e \text{ ( } e \text{ is the electron charge).} \end{aligned} \quad (14)$$

We note that though some of the values  $\delta W_i$  in (14) are negative, the parameter  $W(r-r')_{pq}^f$  in (13) is repulsive (positive) for all separation distances.

The procedure of finding the parameters (14) was performed for the total  $W(r-r')_{pq}$  potential (12) including the strain-induced interaction  $W(r-r')_{pq}^{\text{elast}}$ . The latter was expressed through the phonon Green function and the transformation strain in a way similar to that used before.<sup>1,28,29</sup> In calculating this term we used the new data on the elastic constants  $c_{ij}$  for  $\text{YBa}_2\text{Cu}_3\text{O}_{7-\delta}$  reported in Ref. 31:  $c_{11} \sim 2.3 \times 10^{12}$  dyn/cm<sup>2</sup>,  $c_{12} \sim 1.0 \times 10^{12}$  dyn/cm<sup>2</sup>, and  $c_{66} \sim 0.85 \times 10^{12}$  dyn/cm<sup>2</sup>.

The total potential (12), including  $W(r-r')_{pq}^{\text{elast}}$  and  $W(r-r')_{pq}^f$  with the parameters (14), was used in the computer simulation of oxygen ordering kinetics at stoichiometries  $x < 0.35$ . Some of the results obtained for  $x = 0.25$  are presented in the next section.

Parameters (14) give the following values of the eigenvalues  $\lambda(k)_-$  for the Lifshitz points  $(\frac{1}{2}\frac{1}{2}0)$ ,  $(000)$ , and  $(\frac{1}{2}00)$  at  $x = 0.25$ :

$$\begin{aligned} \lambda(\frac{1}{2}\frac{1}{2}0)_- &= -7610^\circ k_B, \\ \lambda(000)_- &= -4160^\circ k_B, \\ \lambda(\frac{1}{2}00)_- &= -1480^\circ k_B. \end{aligned} \quad (15a)$$

The same functions estimated at  $x = 0.5$  are equal:

$$\begin{aligned} \lambda(\frac{1}{2}\frac{1}{2}0)_- &= -1180^\circ k_B, \\ \lambda(000)_- &= -5190^\circ k_B, \\ \lambda(\frac{1}{2}00)_- &= -1690^\circ k_B. \end{aligned} \quad (15b)$$

In (15b), the value  $\lambda(000)_- = -5190^\circ k_B$  is found by comparing the calculated mean-field transition temperature  $T_0$  of the primary ordering  $T \rightarrow \text{O-I}$  with the observed temperature,  $T_0 \sim 970$  K (Ref. 32) at  $x = 0.5$ . The same value of  $\lambda(000)_-$  was used in the previous works.<sup>1,29</sup> The

value  $\lambda(\frac{1}{2}00)_- = -1690^\circ k_B$  is found by a similar procedure [see Eq. (24) from Ref. 1] consisting in fitting the transition temperature  $T_1$  of the  $\text{O-I} \rightarrow \text{O-II}$  secondary ordering to the observed transition temperature, recently found in the neutron diffuse scattering study,<sup>26</sup>  $T_1 \sim 150^\circ\text{C}$  at  $x = 0.5$ . To find the value  $\lambda(\frac{1}{2}\frac{1}{2}0)_- = -1180^\circ k_B$ , we used the ratio  $\lambda(\frac{1}{2}\frac{1}{2}0)_- / \lambda(\frac{1}{2}00)_- \sim 0.7$ . This ratio was found in Refs. 1, 28, and 29 to provide the right transformation sequence (4) at  $x > 0.5$ .

Comparing Eqs. (15a) and (15b) demonstrates that this is the eigenvalue  $\lambda(\frac{1}{2}\frac{1}{2}0)_-$  that undergoes the most dramatic change somewhere inside the interval  $0.25 < x < 0.5$ . The other eigenvalues,  $\lambda(000)_-$  and  $\lambda(\frac{1}{2}00)_-$ , do not change so much. Such a discriminated effect of the change of the O-O potential on the eigenvalue  $\lambda(\frac{1}{2}\frac{1}{2}0)_-$  proved to be possible due to the anisotropy of the deviations  $\delta W_i$  in Eq. (13). As we see from the obtained parameters Eq. (14), the values  $\delta W_1$  and  $\delta W_3$  (corresponding to the first and third coordination spheres and, thus, representing the O-O pairs along the  $\langle 110 \rangle$  directions) are negative, whereas the values  $\delta W_2$  and  $\delta W_5$  (corresponding to the second and fifth coordination spheres and representing the O-O pairs along the  $\langle 100 \rangle$  directions) are positive (the fourth sphere represents an intermediate direction). This anisotropy contributes to the alignment of oxygen atoms along the  $\langle 110 \rangle$  directions, thus promoting the formation of the  $[110]$  oxygen chain structures in the relevant stoichiometry range (see structures of Fig. 2).

### C. Intermediate range $\sim 0.35 < x < \sim 0.4$

According to Eqs. (15a) and (15b), the decrease in the oxygen concentration from  $x = 0.5$  to  $0.25$  drastically decreases  $\lambda(\frac{1}{2}\frac{1}{2}0)_-$  while insignificantly increasing the values of  $\lambda(000)_-$  and  $\lambda(\frac{1}{2}00)_-$ . The decrease of  $\lambda(\frac{1}{2}\frac{1}{2}0, x)_-$  should change its relation with two other eigenvalues,  $\lambda(000)_-$  and  $\lambda(\frac{1}{2}00)_-$ , which are almost constant. An approximate stoichiometry dependences for the values  $\lambda(\frac{1}{2}\frac{1}{2}0)_-$ ,  $\lambda(000)_-$ , and  $\lambda(\frac{1}{2}00)_-$  are presented in Fig. 4.

It is obvious, that with decrease of  $x$ , the value  $\lambda(\frac{1}{2}\frac{1}{2}0)_- = -1180^\circ k_B$  first drops below the value  $\lambda(\frac{1}{2}00)_-$ . This turns the inequality  $\lambda(\frac{1}{2}\frac{1}{2}0, x)_- > \lambda(\frac{1}{2}00)_-$  into  $\lambda(\frac{1}{2}\frac{1}{2}0, x)_- < \lambda(\frac{1}{2}00)_-$ . Since  $\lambda(\frac{1}{2}\frac{1}{2}0, x)_-$  is still bigger than  $\lambda(000)_-$ , a new relation appears:

$$\lambda(000)_- < \lambda(\frac{1}{2}\frac{1}{2}0)_- < \lambda(\frac{1}{2}00)_-. \quad (16)$$

The point, where  $\lambda(\frac{1}{2}\frac{1}{2}0, x)_- = \lambda(\frac{1}{2}00)_-$ , is marked as point *B* in Fig. 4. Its stoichiometry is probably close to  $x \sim 0.4$  since the orthorhombic  $\text{O-II}$  phase [formed by relations (8)] was still observed at  $x \sim 0.4$ .<sup>24</sup>

When, with a further decrease of  $x$ , the value of  $\lambda(\frac{1}{2}\frac{1}{2}0, x)_-$  also drops below the value of  $\lambda(000)_-$ , then relations (10) become valid. This change, (16) to (10), happens at point *A* in Fig. 4 where  $\lambda(\frac{1}{2}\frac{1}{2}0, x)_- = \lambda(000)_-$ . The stoichiometry of this point is probably close to  $x \sim 0.35$ , since the  $(\frac{1}{4}\frac{1}{4}0)_2$  phase

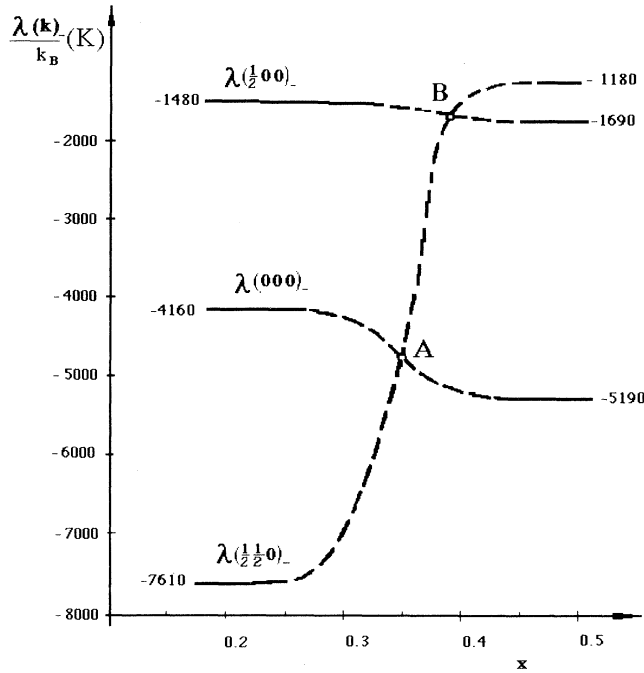


FIG. 4. Approximate stoichiometry dependences of eigenvalues  $\lambda(000)_-$ ,  $\lambda(\frac{1}{2}00)_-$ , and  $\lambda(\frac{1}{2}\frac{1}{2}0)_-$ . The value  $\lambda(\frac{1}{2}\frac{1}{2}0)_- \sim -7610$  K at  $x=0.25$  is found with Eqs. (11a) and (11b) from the assumed transition temperature  $T_0 \sim 830$  K for the  $T \rightarrow (\frac{1}{2}\frac{1}{2}0)_2$  primary ordering transition. The values  $\lambda(000)_- \sim -5190$  K and  $\lambda(\frac{1}{2}00)_- \sim -1690$  K at  $x=0.5$  are found from the observed temperatures [ $T_0 \sim 970$  K (Ref. 33) and  $T_1 \sim 420$  K (Ref. 26)] of the  $T \rightarrow$ O-I and O-I  $\rightarrow$  O-II transitions, respectively. The intermediate stoichiometry region around  $x=0.4$  corresponds to the intermediate relations [Eq. (16)] between the three main eigenvalues  $\lambda(\mathbf{k})_-$ .

[formed by relations (10)] was observed at  $x \sim 0.35$ .<sup>2</sup>

Therefore, the experimental data<sup>2,24</sup> imply that relations (16) may realize approximately between  $x \sim 0.35-0.36$  and  $x \sim 0.39-0.40$  (points A and B in Fig. 4). This estimate is in agreement with the neutron-diffraction study<sup>23</sup> demonstrating that the orthorhombic-to-tetragonal and superconductor-to-semiconductor transitions happen near  $x \sim 0.35$  (and certainly between

$x=0.34$  and  $0.38$ ). Similar results were obtained in Ref. 33.

#### IV. CONCENTRATION WAVE ANALYSIS OF ORDERED STRUCTURES WITHIN THE INTERMEDIATE RANGE

$$\sim 0.35 < x < \sim 0.4$$

In this range the primary ordering is dictated by inequalities (16). It results in the same  $T \rightarrow$ O-I transition that is observed at  $x > 0.4$  [where relations (8) are valid]. This happens because in both regions  $\lambda(000)_- = \min[\lambda(\mathbf{k})_-]$ . The occupation probabilities describing the O-I phase are given by the function

$$n(p, \mathbf{r})_0 = \begin{cases} n(1, \mathbf{r})_0 = c + \eta_0, \\ n(2, \mathbf{r})_0 = c - \eta_0, \end{cases} \quad (17)$$

where  $\eta_0$  is the LRO parameter related to the antisymmetric representation of the group of the wave vector  $\mathbf{k}=0$ . The  $c \pm \eta_0$  terms, describing the preferred occupation by O atoms of the first sublattice, also enter Eqs. (1b) and (2b) describing the  $(\frac{1}{2}\frac{1}{2}0)_1$  and  $(\frac{1}{4}\frac{1}{4}0)_1$  phases.

According to relations (16), the secondary ordering is generated by the concentration wave  $\mathbf{k}_0 = (2\pi/a_0)(\frac{1}{2}\frac{1}{2}0)$ . To find the corresponding function  $n(p, \mathbf{r})_2$  describing the secondary ordered phase, this concentration wave has to be added to function (17) so that the resultant  $n(p, \mathbf{r})_2$  would meet the stability criteria<sup>19,20</sup> presented in the Appendix. This function is given by Eq. (1b). It produces the orthorhombic  $(\frac{1}{2}\frac{1}{2}0)_1^{\text{centr}}$  secondary ordered phase shown in Fig. 2(b) with a  $2a_0 \times 2a_0$  centered unit cell (O atoms occupy only one of two sublattices in the completely ordered state). The stoichiometry of this phase is  $x=2c=0.5$ . Since within the relevant range  $\lambda(\frac{1}{2}\frac{1}{2}0)_- < \lambda(\frac{1}{2}00)_-$ , this  $(\frac{1}{2}\frac{1}{2}0)_1^{\text{centr}}$  phase is energetically more favorable than the O-II structure (generated by the  $\{\frac{1}{2}00\}$  concentration waves).

However, since the stoichiometry of this  $(\frac{1}{2}\frac{1}{2}0)_1^{\text{centr}}$  phase,  $x=0.5$ , is outside the relevant range, it should undergo the tertiary ordering with the decrease of temperature. This tertiary ordering is generated by the "second best" concentration waves  $\{\frac{1}{2}00\}$  competing with the  $(\frac{1}{2}\frac{1}{2}0)$  wave in relations (16). The tertiary ordered phase is described by the equation

$$n(p, \mathbf{r})_3 = \begin{cases} n(1, \mathbf{r})_3 = c + \eta_0 + (\eta_1 + \eta'_1) \exp(i\mathbf{k}_0 \mathbf{r}) + (\eta_2 + \eta'_2) [\cos(\mathbf{k}'_2 \mathbf{r}) + \cos(\mathbf{k}''_2 \mathbf{r})], \\ n(2, \mathbf{r})_3 = c - \eta_0 + (\eta_1 - \eta'_1) \exp(i\mathbf{k}_0 \mathbf{r}) + (\eta_2 - \eta'_2) [\cos(\mathbf{k}'_2 \mathbf{r}) + \cos(\mathbf{k}''_2 \mathbf{r})], \end{cases} \quad (18)$$

where  $\mathbf{k}'_2 = (2\pi/a_0)(0\frac{1}{2}0)$  and  $\mathbf{k}''_2 = (2\pi/a_0)(\frac{1}{2}00)$ ;  $\eta_2$  and  $\eta'_2$  are the LRO parameters related to the symmetric and antisymmetric irreducible representations of the groups of the wave vectors  $\mathbf{k}'_2$  and  $\mathbf{k}''_2$ , respectively. The completely ordered state is achieved if  $c = \eta_0 = \eta_1 = \eta'_1 = \eta_2 = \eta'_2 = \frac{1}{8}$ . Therefore, its ideal stoichiometry  $x=2c=0.25$  is also outside the relevant range. Within this range, this phase can be formed only as a nonstoichiometric precursor of a quaternary ordered phase.

The structure of the tertiary phase, described by Eq. (18), is shown in Fig. 5(c). It also has a  $2a_0 \times 2a_0$  unit cell. But this cell is primitive. Since oxygen atoms preferentially occupy one of the two interstitial sublattices, this structure is orthorhombic. To reflect these characteristics, we designate this phase  $(\frac{1}{2}\frac{1}{2}0)_1^{\text{prim}}$ . The diffraction pattern corresponding to the  $(\frac{1}{2}\frac{1}{2}0)_1^{\text{prim}}$  phase was observed by Reyes-Gasga *et al.*<sup>7</sup> It is distinguished from the diffraction pattern of the  $(\frac{1}{2}\frac{1}{2}0)_1^{\text{centr}}$  phase by the presence of the  $\{\frac{1}{2}00\}$ -type reflections.

To find the concentration waves generating the quaternary ordered phase at low temperatures, we have to take into consideration the fact that the  $\{\frac{1}{4}\frac{1}{4}0\}$  waves participate in formation of the low-temperature ordered phases on both sides of the  $0.35 < x < 0.4$  interval, i.e., at  $x < 0.35$  and  $x > 0.4$ . Thus, it is natural to assume that the same star is operational within the  $0.35 < x < 0.4$  range. Constructing the occupation probability function, by adding the concentration waves  $\{\frac{1}{4}\frac{1}{4}0\}$  in such a way that the resultant function  $n(p, r)_4$  would meet the stability criteria (see the Appendix), we have the atomic distribution for the quaternary ordered phase:

$$n(p, r)_4 = \begin{cases} n(1, r)_4 \\ n(2, r)_4 \end{cases} = \begin{cases} c + \eta_0 + (\eta_1 + \eta_1)\exp(i\mathbf{k}_0\mathbf{r}) + (\eta_2 + \eta'_2)[\cos(\mathbf{k}'_2\mathbf{r}) + \cos(\mathbf{k}''_2\mathbf{r})] + (\eta_3 + \eta'_3)[\cos(\mathbf{k}'_3\mathbf{r}) + \cos(\mathbf{k}''_3\mathbf{r})] \\ c - \eta_0 + (\eta_1 - \eta'_1)\exp(i\mathbf{k}_0\mathbf{r}) + (\eta_2 - \eta'_2)[\cos(\mathbf{k}'_2\mathbf{r}) + \cos(\mathbf{k}''_2\mathbf{r})] + (\eta_3 - \eta'_3)[\cos(\mathbf{k}'_3\mathbf{r}) + \cos(\mathbf{k}''_3\mathbf{r})] \end{cases}, \quad (19)$$

where  $\mathbf{k}'_3 = (2\pi/a_0)(\frac{1}{4}\frac{1}{4}0)$  and  $\mathbf{k}''_3 = (2\pi/a_0)(\frac{3}{4}\frac{3}{4}0)$ ,  $\eta_3$  and  $\eta'_3$  are the LRO parameters related to the symmetric and antisymmetric irreducible representations of the groups of the vectors  $\mathbf{k}'_3$  and  $\mathbf{k}''_3$ . It is interesting that this function is able to describe the ordered structures of the same symmetry but with different stoichiometries. One of them is of particular interest because its ideal stoichiometry is inside the range  $0.35 < x < 0.4$ . This stoichiometry is achieved if  $c = \eta_0 = \eta_1 = \eta'_1 = \frac{3}{16}$ ,  $\eta_2 = \eta'_2 = -\frac{1}{16}$ ,  $\eta_3 = \eta'_3 = \frac{1}{8}$ . With these values, the function  $n(p, r)_4$  given by Eq. (19) assumes only two values, either 1 or 0. Placing O atoms at the interstitial sites  $\{p, r\}$  where the function  $n(p, r)_4$  assumes the value 1, we obtain the completely ordered structure shown in Fig. 5(d). Its stoichiometry  $x = 2c = \frac{3}{8} = 0.375$ .

Therefore, the function  $n(p, r)_4$  describes the ultimate ordered phase which at low temperatures does not undergo the further ordering. Thus, this phase could be observed within the relevant range,  $0.35 < x < 0.4$ . It is one of the  $(\frac{1}{4}\frac{1}{4}0)_1$  orthorhombic phases with a  $2\sqrt{2}a_0 \times 2\sqrt{2}a_0$  unit cell. This phase is named below as  $\gamma - (\frac{1}{4}\frac{1}{4}0)_1$ . Its atomic structure is given in Fig. 5(d). The diffraction pattern of this phase coincides with that shown in Fig. 1(c). The same diffraction pattern was found by Rayes-Gasga *et al.*<sup>7</sup> What is important is that, in an agreement with our analysis, these authors also observed the  $(\frac{1}{2}\frac{1}{2}0)_1^{\text{prim}}$  phase as a precursor of the  $\gamma - (\frac{1}{4}\frac{1}{4}0)_1$  phase. The same  $\gamma - (\frac{1}{4}\frac{1}{4}0)_1$  ordered phase was also reported in the neutron-diffraction study<sup>13</sup> (for a close stoichiometry  $x \sim 0.35$ ). We note, that this ordered structure was suggested, as one of several possible ground-state structures at  $x = \frac{3}{8}$ , in the analysis<sup>22,34</sup> based on screened-Coulomb O-O interaction.

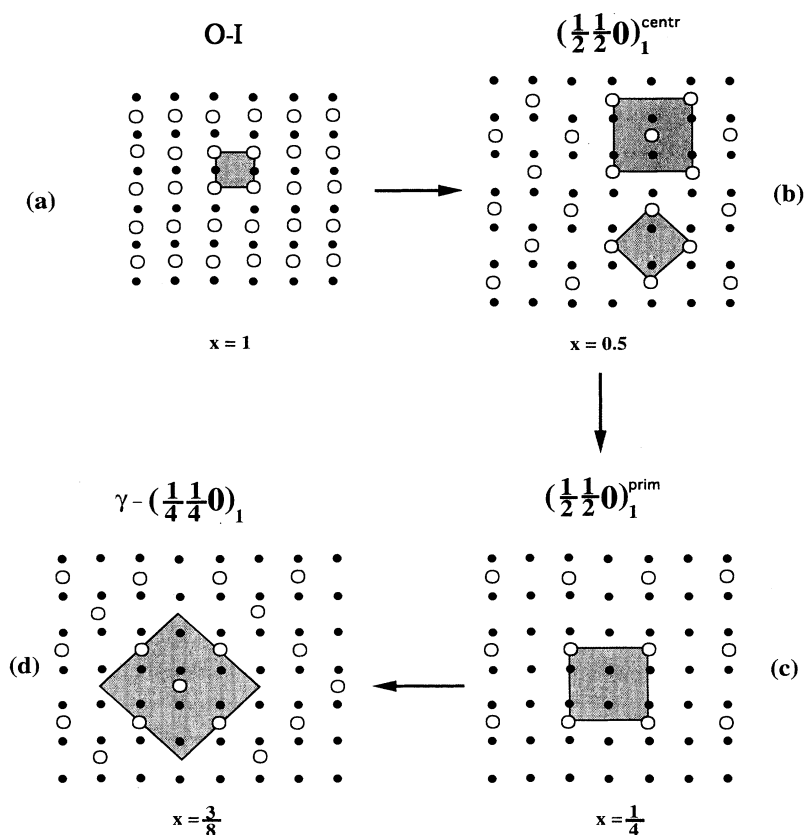
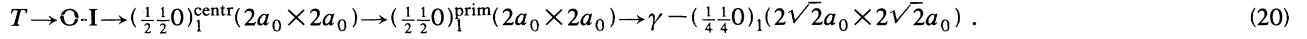


FIG. 5. The family of orthorhombic superstructures, described by Eqs. (17), (1b), (18), and (19) [the structures (a)–(d), respectively] which are the derivatives of the O-I phase within the intermediate range  $\sim 0.35 < x < \sim 0.4$ . The  $(\frac{1}{2}\frac{1}{2}0)_1^{\text{prim}}$  phase (c) was observed (Ref. 7) as a precursor of the  $\gamma - (\frac{1}{4}\frac{1}{4}0)_1$  ( $2\sqrt{2}a_0 \times 2\sqrt{2}a_0$ ) phase (d). The diffraction of the  $\gamma - (\frac{1}{4}\frac{1}{4}0)_1$  ( $2\sqrt{2}a_0 \times 2\sqrt{2}a_0$ ) phase [Fig. 1(c)] was found in Refs. 7 and 13.

Summing up the above results, the following sequence of ordering reactions at cooling the tetragonal  $T$  phase can be predicted within the interval  $0.35 < x < 0.4$ :



Therefore, the change of the O-O interaction with the decrease in stoichiometry from  $x = 0.5$  to  $0.25$  results in the relative change of the eigenvalues  $\lambda(000)_-$ ,  $\lambda(\frac{1}{2}\frac{1}{2}0)_-$ , and  $\lambda(\frac{1}{2}00)_-$  transforming inequality (8) into (16) and then into (10). Upon decrease in stoichiometry the sequences (4), (20), and (3) are successively observed.

### V. COMPUTER SIMULATIONS OF OXYGEN ORDERING AT $x = 0.25$

The O-O interaction potential, described by Eqs. (12) and (13) with the parameters (14), allows us to carry out the computer simulation of the structure transformation kinetics during the multiple ordering at the stoichiometry  $x = 0.25$  [at which the parameters (14) were found] and at close stoichiometries where we do not expect for the O-O potential to change considerably. We present below the results of the computer simulation for  $x = 0.25$ .

The simulation method, based on the numerical solution of the nonlinear crystal-lattice-site diffusion equation, is exactly the same as that used before.<sup>1,28,29</sup> Since it was described in full detail in Ref. 1, we do not repeat it here. The only change made is the introduction of the “random noise” fluctuations, meeting the requirement of the fluctuation-dissipation theorem, into the microscopic diffusion kinetic equations and, thus, effectively transforming them into the stochastic Langevin equations. The fluctuations allow a system to avoid trapping in free-energy local minima (metastable states) which is essential since most of the phase transformations related to formation of the  $\{\frac{1}{4}\frac{1}{4}0\}$  phases are the first-order transitions. The Langevin microscopic diffusion equation is

$$\frac{dn(p, \mathbf{r}; t)}{dt} = \sum_{q=1}^{q=2} \sum_{\mathbf{r}'} L(\mathbf{r} - \mathbf{r}')_{pq} \frac{\delta F}{\delta n(q, \mathbf{r}'; t)} + \xi_p(\mathbf{r}, t), \quad (21)$$

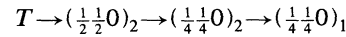
where  $n(p, \mathbf{r}; t)$  is the same function of the occupation probability that is used in the above analysis,  $t$  is the time. The function  $L(\mathbf{r} - \mathbf{r}')_{pq}$  is the matrix of the kinetic coefficients which are the typical inverse times of an elementary diffusional jump from the site  $(q, \mathbf{r}')$  to the site  $(p, \mathbf{r})$ . The variational derivative,  $\delta F / \delta n(q, \mathbf{r}'; t)$ , is the transformation driving force;  $\xi_p(\mathbf{r}, t)$  is a random noise meeting the requirement of the fluctuation-dissipation theorem. The summation over  $\mathbf{r}'$  is carried out over all  $N$  unit cells of the crystal.

As before, oxygen ordering was described with the Ising model allowing all structure states to be obtained by the O atoms redistribution over interstitial sites of two sublattices  $(p, q = 1, 2)$  located in a basal Cu(1)-O(001) plane of  $\text{YBa}_2\text{Cu}_3\text{O}_{6+x}$ . Equation (21) was formulated in a dimensionless form using the reduced time  $t^* = t/\tau$ , where  $\tau = (4AL_1)^{-1}$  is the typical time of an elementary diffusion event,  $L_1$  is the kinetic coefficient  $L(\mathbf{r} - \mathbf{r}')_{pq}$  for the nearest-neighbor diffusional jump,  $A = (z^*)^2 / (a_0/\sqrt{2})$  [see Eq. (13)]. The simulation of the oxygen or-

dering kinetics was realized by numerical solution of the kinetic equation (21) with the periodical boundary conditions. The computational cell consists of the  $64 \times 64$  unit cells in the Cu(1)-O(001) basal plane. The computer-simulation results are presented in Figs. 6 and 7.

The oxygen-ordering kinetics was simulated by “quenching” the disordered tetragonal  $T$  phase to a temperature  $T_a$ , which is below the order-disorder transition temperature  $T_0$  for the  $T \rightarrow (\frac{1}{2}\frac{1}{2}0)_2$  transition, and subsequent “annealing” at  $T_a$  and more low temperatures. The simulations at different temperatures  $T_a$  have shown that the  $(\frac{1}{2}\frac{1}{2}0)_2$  phase forms only in the very beginning of evolution at any temperature  $T_a$ , i.e., the transition temperature  $T_0$  practically coincides with the next transition temperature  $T_1$  for the secondary  $(\frac{1}{2}\frac{1}{2}0)_2 \rightarrow (\frac{1}{4}\frac{1}{4}0)_2$  ordering. However, the tertiary transition  $(\frac{1}{4}\frac{1}{4}0)_2 \rightarrow (\frac{1}{4}\frac{1}{4}0)_1$  has a significantly lower transition temperature  $T_2 \sim 0.7 \times T_0$  at  $x = 0.25$ .

Figures 6(a)–6(c) demonstrate the evolution of atomic and mesoscale structures formed at multiple ordering



[sequence (3)]. Figures 6(a) and 6(b) show the structures corresponding to the “short” and “long” annealing times (the reduced time  $t^* = 60$  and  $420$ , respectively) at a comparatively high-temperature  $T_a = 0.95 \times T_0$  [ $T_0 = 830$  K at  $x = 0.25$ , see Eqs. (11)]. Figure 6(a) ( $t^* = 60$ ) presents the mixture of two orientation variants of the metastable  $(\frac{1}{2}\frac{1}{2}0)_1^{\text{centr}}$  phase which starts to transform into the stable  $(\frac{1}{4}\frac{1}{4}0)_2$  phase [these structures are shown in Figs. 2(b) and 2(c)]. However, residues of the primary ordered  $(\frac{1}{2}\frac{1}{2}0)_2$  phase can be seen in Fig. 6(a) as the one-line oxygen chains in  $\langle 110 \rangle$  directions located mostly on interfacial boundaries. This  $(\frac{1}{2}\frac{1}{2}0)_2$  phase [see Fig. 2(a)] forms only in the very beginning of the transformation, rapidly transforming into the transient  $(\frac{1}{2}\frac{1}{2}0)_1^{\text{centr}}$  structure. The latter transforms much more slowly into the stable secondary ordered  $(\frac{1}{4}\frac{1}{4}0)_2$  phase. This evolution is easily seen by comparison of Figs. 6(a) and 6(b).

Figure 6(b) ( $t^* = 420$ ) demonstrates only one phase, the  $(\frac{1}{4}\frac{1}{4}0)_2$  ( $\sqrt{2}a_0 \times 2\sqrt{2}a_0$ ) ordered structure in two orientation variants with the antiphase domains within each variant. This is the structure that was found by Zeiske *et al.*<sup>2</sup> in a sample with  $x \sim 0.35$ . Its diffraction pattern coincides with that in Fig. 1(a). Since further annealing ( $t^* > 420$ ) practically does not change this structure, it is the stable equilibrium structure at  $T_a = 0.95 \times T_0$ .

This structure was then slowly “cooled” (in nine steps, during the reduced time  $t^* = 270$ ) to the lower temperature  $T_a = 0.4 \times T_0$  which is below the transition temperature  $T_2$  for the  $(\frac{1}{4}\frac{1}{4}0)_2 \rightarrow (\frac{1}{4}\frac{1}{4}0)_1$  transition ( $T_2 \approx 0.7 \times T_0$  at  $x = 0.25$ ). The obtained low-temperature structure,

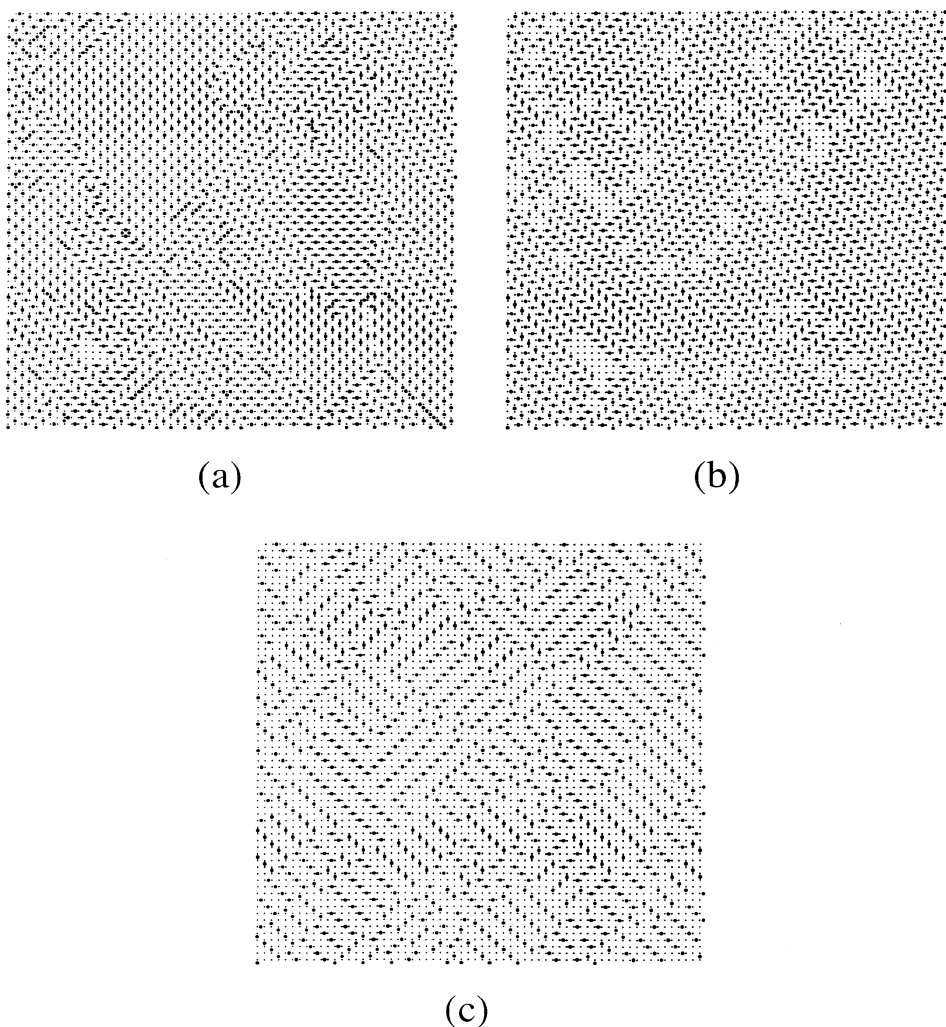


FIG. 6. Simulated microstructures for  $\text{YBa}_2\text{Cu}_3\text{O}_{6.25}$  obtained by “quenching” and “annealing” the tetragonal  $T$  phase. The model crystal consists of  $64 \times 64$  computational cells. Oxygen atoms (large solid circles) are shown in interstitial positions  $(p, r)$  if the occupation probability  $n(p, r; t) > c = 0.125$ . Small points are the Cu atoms. (a) Reduced time  $t^* = 60$  and  $T/T_0 = 0.95$ ; (b) reduced time  $t^* = 420$  and  $T/T_0 = 0.95$ . (c) The structure (b) after additional slow “cooling” to  $T/T_0 = 0.4$ . Temperature  $T_0 \sim 830$  K is the temperature of the  $T \rightarrow (\frac{1}{2} \frac{1}{2})_2$  transition.  $T/T_0 = 0.4$  is below the temperature of the  $(\frac{1}{4} \frac{1}{4})_2 \rightarrow (\frac{1}{4} \frac{1}{4})_1$  transition. (a) shows two orientation variants of the metastable  $(\frac{1}{2} \frac{1}{2})_1^{\text{centr}}$  ( $2a_0 \times 2a_0$ ) phase and the stable secondary ordered  $(\frac{1}{4} \frac{1}{4})_2$  phase as well as the traces of the primary ordered structure  $(\frac{1}{2} \frac{1}{2})_2$ . (b) shows two orientation variants of the stable  $(\frac{1}{4} \frac{1}{4})_2$  structure and the antiphase domains within each variant. (c) shows the domains of the tertiary ordered  $(\frac{1}{4} \frac{1}{4})_1$  phase.

presented in Fig. 6(c), is the tertiary ordered  $(\frac{1}{4} \frac{1}{4})_1$  ( $\sqrt{2}a_0 \times 2\sqrt{2}a_0$ ) structure [see Fig. 2(c)]. We found that this structure is also the stable equilibrium structure since it does not practically change with the further annealing at the same and more low temperatures.

Figure 6(c) shows two orientation variants of  $(\frac{1}{4} \frac{1}{4})_1$

( $\sqrt{2}a_0 \times 2\sqrt{2}a_0$ ) structure and the antiphase domains within each of them. This structure was suggested by Kemin *et al.*<sup>3</sup> Its diffraction pattern coincides with that in Fig. 1(b).

The simulated diffraction patterns, corresponding to the structures presented in Figs. 6(b) and 6(c), are shown

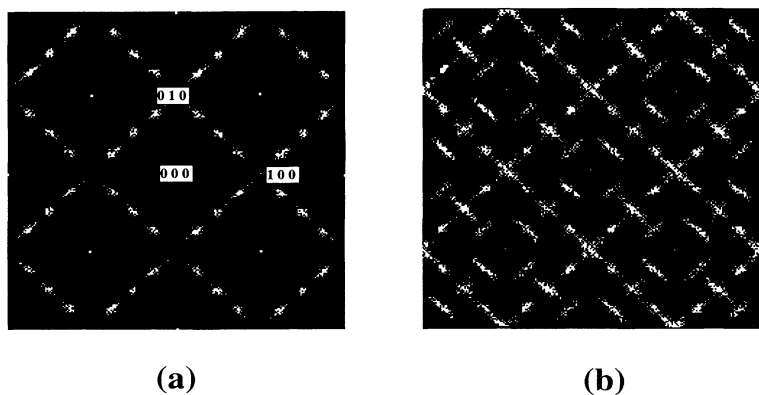


FIG. 7. Simulated diffraction patterns. (a) The pattern from the  $(\frac{1}{4} \frac{1}{4})_2$  structure shown in Fig. 6(b); (b) the pattern from the  $(\frac{1}{4} \frac{1}{4})_1$  structure, shown in Fig. 6(c). Both patterns (a) and (b) are generated by two orientation variants of the corresponding structure. All intensities are given in the logarithmic scale. Three fundamental maxima, (000), (100), and (010), are marked in (a).

in Figs. 7(a) and 7(b), respectively. Besides the superstructure maxima, corresponding to two orientation variants of  $(\frac{1}{4}\frac{1}{4}0)_2$  and  $(\frac{1}{4}\frac{1}{4}0)_1$  ordered structures, the patterns contain the fundamental maxima. Since the width of fundamental maxima is negligible (it coincides with an increment in the  $\mathbf{k}$  space), and the intensities are given in the logarithmic scale, they are hardly visible and therefore three of them are marked in Fig. 7(a).

Comparing the simulated diffractions of Figs. 7(a) and 7(b) with the observed diffraction patterns of Figs. 1(a) and 1(b) shows that the simulated diffraction is just a superposition of diffractions from two orientation variants.

Therefore, the computer simulation of the multiple oxygen ordering at  $x=0.25$  with O-O potentials (12)–(14) generates the same oxygen superstructures, the  $(\frac{1}{4}\frac{1}{4}0)_2$  and  $(\frac{1}{4}\frac{1}{4}0)_1$  ordered phases with the  $\sqrt{2}a_0 \times 2\sqrt{2}a_0$  unit cell, which were observed by Zeiske *et al.*<sup>2</sup> and Kemin *et al.*<sup>3</sup>

## VI. DISCUSSION

The analysis of available diffraction data, the concentration-wave analysis of ordering and the computer simulation, taken together, enable one to establish the main features of the general picture of complicated ordering transformations in  $\text{YBa}_2\text{Cu}_3\text{O}_{6+x}$  system. Controversies in interpretation of experimental results are mostly caused by the fact that these transformations are very different from the conventional replace transformations involving the ordering. Two major factors contribute to this difference.

(1) The first one is the dominance of the long-range repulsive O-O interaction which suppresses the conventional mechanism of establishing the ideal stoichiometry at low temperatures, viz., the decomposition into a mixture of macroscopic volumes of the fully ordered phases with ideal stoichiometries. If such a decomposition mechanism is suppressed, which is the case for the  $\text{YBa}_2\text{Cu}_3\text{O}_{6+x}$  system, then the stoichiometry can be achieved upon cooling only by the sequence of secondary, tertiary, and so on ordering reactions. In principle, these structure changes have to occur until the ideal stoichiometry of the resultant phase becomes equal to the current overall stoichiometry  $x$  of the system. In other words, each current stoichiometry should result in the corresponding ground-state structure, different for each stoichiometry. Well-known examples of such ground-state structures are the devil's staircase structures in a  $\text{YBa}_2\text{Cu}_3\text{O}_{6+x}$  system with the screened Coulomb O-O interaction was demonstrated by Adelman *et al.*<sup>35</sup> using the Monte Carlo simulation and by Aligia *et al.*<sup>34</sup> using the ground-state analysis.

In most cases, however, there are the kinetic and thermodynamic reasons preventing the complete realization of this ideal scenario. Although each consecutive ordering occurring upon coolings brings an ideal stoichiometry of the current ordered phase closer to the overall stoichiometry, but it simultaneously reduces the transformation driving force and slows down the diffusional kinetics. This makes the each next ordering reaction

more and more sluggish. The slowing down of the ordering kinetics occurs until one of the transient ordered phases turns out to be frozen.

Since the repulsive long-range character of the O-O interaction suppresses the decomposition, the composition  $x$  is not a degree of freedom. Therefore, the Gibbs phase rule predicts that the stability fields of different ordered phases, as in the case of the diffusionless transformation, should be separated by a line rather than by an intervening two-phase region. The latter actually explains why all attempts to observe a two-phase state in the  $\text{YBa}_2\text{Cu}_3\text{O}_{6+x}$  system still have not produced any conclusive result. It should also be mentioned that any short-range interaction model for the O-O potential should always result in a diagram with two-phase fields.

(2) The second factor contributing to the complexity of ordering is the drastic change of the O-O interaction potentials within a narrow concentration range  $\sim 0.3 < x < \sim 0.45$  (Fig. 4), where the electron structure of the system undergoes the radical reconstruction, transforming the high-temperature superconducting state into

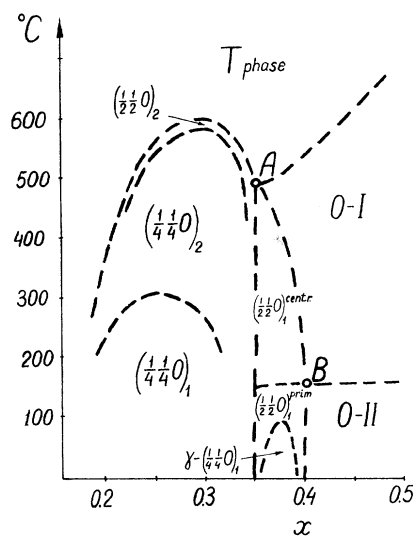


FIG. 8. Approximate position of the stability fields of the  $T$ ,  $(\frac{1}{2}\frac{1}{2}0)$  and  $\{\frac{1}{4}\frac{1}{4}0\}$  ordered phases illustrating the sequences of oxygen ordering phase transformations in substoichiometric  $\text{YBa}_2\text{Cu}_3\text{O}_{6+x}$  upon cooling [Eqs. (22b) and (22c)]. The temperature of the  $T \rightarrow (\frac{1}{2}\frac{1}{2}0)_2$  transition at  $x=0.25$  is assumed to be around of the observed values, i.e., between 500 and 600 °C (Refs. 14 and 15). The  $(\frac{1}{4}\frac{1}{4}0)_2 \rightarrow (\frac{1}{4}\frac{1}{4}0)_1$  transition temperature at  $x=0.25$  is obtained in the computer simulation with the O-O potential (12)–(14). Points A and B, corresponding to the borders of the intermediate region  $0.35 < x < 0.4$  are defined in Fig. 4. The O-I  $\rightarrow$  O-II transition temperature near point B is indicated in accordance with the experimental value  $\sim 150$  °C (Ref. 26). The diffractions from the  $(\frac{1}{4}\frac{1}{4}0)_2$  and  $(\frac{1}{4}\frac{1}{4}0)_1$  phases with a  $\sqrt{2}a_0 \times 2\sqrt{2}a_0$  unit cell, shown in Figs. 1(a) and 1(b), respectively, were observed in Refs. 2 and 3. The diffraction from the  $\gamma$ - $(\frac{1}{4}\frac{1}{4}0)_1$  ( $2\sqrt{2}a_0 \times 2\sqrt{2}a_0$ ) phase, shown in Fig. 1(c), was observed in Refs. 7 and 13. The  $(\frac{1}{2}\frac{1}{2}0)_1^{\text{prim}}$  phase was observed in Ref. 7 as a precursor of the  $\gamma$ - $(\frac{1}{4}\frac{1}{4}0)_1$   $2\sqrt{2}a_0 \times 2\sqrt{2}a_0$  phase.

a semiconducting state and abruptly changing different physical properties.<sup>18,23</sup> This change of the O-O potentials have to be large enough to alternate the sequence of ordering transformations in different concentration ranges.

There is one circumstance that has to be taken into account in interpretation of diffraction data for the  $(\frac{1}{4}\frac{1}{4}0)$  phases. This is the effect of atomic displacements on the diffraction intensities caused by interstitial O atoms in basal Cu-O planes. Particularly, there are many indications that the atomic displacements significantly affect the intensity of the  $\{\frac{1}{4}\frac{1}{4}0\}$  superlattice reflections (see, for example, Ref. 2). This effect may sometimes be confusing and lead to the assumption that these phases are formed as a result of the displacive transformation. However, it should be born in mind that the interstitial oxygen produces the atomic displacements of heavy cations, Cu, Ba, and Y. The concentration waves, describing the atomic distribution of O atoms, generate the displacive waves of cations of the same wave vector which, in turn, contribute to the intensities of superlattice reflections corresponding to these wave vectors. The contribution of the displacements can be very considerable and, in some cases, dominant since the cross section of scattering by heavy cations is much higher than that of the O atoms. Therefore, the large contribution of the displacements of cations to the intensities of superlattice spots is not neces-

sarily a manifestation of the displacive transformation. The oxygen ordering produces these displacements as well.

The existing interpretations of ordering in the  $\text{YBa}_2\text{Cu}_3\text{O}_{6+x}$  system are sometimes sketchy and often contradictory because of its unusual complexity and also the fact that the main part of the structural information on the multiple ordering is based on the thin-film selected-area electron diffraction rather than on the regular analysis of intensities of reflections in the bulk single-crystal diffraction patterns (exceptions are the works in Refs. 2, 13, 24, 26, and 36). The concentration-wave stability analysis, combining the symmetry and thermodynamics arguments, as well as the computer-simulation data on the ordering kinetics presented in this study, actually allow one to recover a part of the missing structure information and construct a rough general picture of ordering in  $\text{YBa}_2\text{Cu}_3\text{O}_{6+x}$  system. This picture seems to be consistent with existing observations and certainly could be modified and made more accurate with appearance of new experimental data.

According to this study, there are three concentration intervals where the sequence of ordering reactions upon cooling is different. They are separated by stoichiometries  $x_A \sim 0.35$  and  $x_B \sim 0.4$  (see Figs. 4 and 8).

(i) At  $x > x_B$ , depending on kinetics, the sequence is either

$$T \rightarrow \text{O-I} \rightarrow \text{O-II (or O-II "glassy" state)} \rightarrow \alpha\text{- or } \beta\text{-}(\frac{1}{4}\frac{1}{4}0)_1(2\sqrt{2}a_0 \times 2\sqrt{2}a_0)$$

[Eq. (4) and Fig. 3] or

$$T \rightarrow \text{O-I} \rightarrow \text{O-II "glassy" state} \rightarrow \text{Magneli-like states} . \quad (22a)$$

(ii) At  $x_A < x < x_B$ , it is

$$T \rightarrow \text{O-I} \rightarrow (\frac{1}{2}\frac{1}{2}0)_1^{\text{centr}}(2a_0 \times 2a_0) \rightarrow (\frac{1}{2}\frac{1}{2}0)_1^{\text{prim}}(2a_0 \times 2a_0) \rightarrow \gamma\text{-}(\frac{1}{4}\frac{1}{4}0)_1(2\sqrt{2}a_0 \times 2\sqrt{2}a_0) \quad (22b)$$

[Eq. (20) and Fig. 5].

(iii) At  $x < x_A$ , it is

$$T \rightarrow (\frac{1}{2}\frac{1}{2}0)_2 \rightarrow (\frac{1}{4}\frac{1}{4}0)_2(\sqrt{2}a_0 \times 2\sqrt{2}a_0) \rightarrow (\frac{1}{4}\frac{1}{4}0)_1(\sqrt{2}a_0 \times 2\sqrt{2}a_0) \quad (22c)$$

[Eq. (3) and Fig. 2].

The O-II "glassy" state entering Eq. (22a) is the short-range-order state consisting of ultrafine domains of the O-II phase. Equations (22b) and (22c) present the sequences of oxygen-ordering phase transformations upon cooling the tetragonal  $T$  phase which can be expected at small  $x$ , within the "tetragonal" part of the phase diagram. These sequences, together with the computer-simulation results at  $x=0.25$ , allow us roughly indicate the mutual position of stability fields of ordered phases entering Eqs. (22b) and (22c). This is schematically shown in Fig. 8 (the position of the O-I  $\rightarrow$  O-II transition line at larger stoichiometries  $x > 0.4$  is drawn according to the observed transformation temperature  $\sim 150^\circ\text{C}$ .<sup>26</sup> In accordance with the foregoing discussion, the two-phase fields which are supposed to be suppressed by the Coulomb repulsion are not shown. Thus, Fig. 8 schematically summarizes main results obtained in this study on

the phases transformations occurring at small  $x$ . These results were obtained from the concentration-wave analysis, available diffraction data, and the computer-simulation analysis. We believe that to some extent these results may give a guideline in future experimental studies of the phase diagram. The obtained results also allow us to make certain conclusions about the structure of ordered phases and their structural relation at  $x < x_A$  and  $x_A < x < x_B$ .

## VII. CONCLUSIONS

(1) The concentration-wave analysis based on the available experimental data results in the conclusion that there are two families of ordered phases in  $\text{YBa}_2\text{Cu}_3\text{O}_{6+x}$  oxides. The ordered phases belonging to the first family are the structural derivatives of the orthorhombic O-I phase generated by the (000) Lifshitz star. They are

formed at  $x > x_A \sim 0.35$ . The ordered phases belonging to the second family are the structural derivatives of the pseudotetragonal  $(\frac{1}{2}\frac{1}{2}0)_2$  primary ordered phase generated by the  $(\frac{1}{2}\frac{1}{2}0)$  Lifshitz star. They are formed at  $x < x_A$ .

(2) It is found that the explanation of ordered structures observed in different concentration ranges requires an assumption that the O-O interaction potential undergoes an abrupt change within the narrow concentration interval  $\sim 0.30 < x < 0.4$ .

(3) The long-range repulsive electrostatic interaction rules out the appearance of two-phase fields in the phase diagram. The single-phase stability fields in the phase diagram are separated by single equilibrium lines. Under these circumstances, the system cooling results in a sequence of multiple ordering reactions bringing the stoichiometries of the ordered phases closer to the overall stoichiometry. The structures of the  $\{\frac{1}{2}\frac{1}{2}0\}$  and  $\{\frac{1}{4}\frac{1}{4}0\}$  phases and the sequences of ordering reactions at cooling the tetragonal  $T$  phase are found (the latter are schematically illustrated by Fig. 8).

(4) Computer simulation of oxygen ordering at  $x = 0.25$  is carried out. It demonstrates the microstructure evolution during the ordering which produces the atomic and domain structures of the  $(\frac{1}{4}\frac{1}{4}0)_2$  and  $(\frac{1}{4}\frac{1}{4}0)_1$  phases with a  $\sqrt{2}a_0 \times 2\sqrt{2}a_0$  unit cell [Figs. 6(a)–6(c)]. Simulated diffraction patterns (Fig. 7) from these phases coincide with the observed diffractions [Figs. 1(a) and 1(b)] if two orientation variants of ordered domains are taken into account.

#### ACKNOWLEDGMENTS

We gratefully acknowledge the support by Division of Materials Science, U.S. Department of Energy, under Grant No. DE-FG05-90ER45430. The simulation was performed on the Cray-YMP 90 at the Pittsburgh Supercomputing Center. We are grateful to Yunzhi Wang for his help.

#### APPENDIX

The possible structures of ordered phases can be found by using the concentration-wave method.<sup>19,20</sup> Any occupation probability function  $n(p, \mathbf{r})$  describing an ordered structure can always be presented as a superposition of the concentration waves, the eigenfunctions  $\phi(p, \mathbf{r})_{s, \mathbf{k}} = v(p, \mathbf{k})_s \exp(i\mathbf{k}\mathbf{r})$  of the matrix  $W(\mathbf{r} - \mathbf{r}')_{pq}$ , where  $s = 1, 2$  numbers two branches of its spectrum  $\lambda(\mathbf{k})_{\pm}$ , the coefficients  $v(p, \mathbf{k})_s$  are the eigenfunctions of the  $2 \times 2$  matrix  $V(\mathbf{k})_{pq}$  in Eq. (5). Without a loss of generality, the function  $n(p, \mathbf{r})$  can be written as

$$n(p, \mathbf{r}) = c + \sum_{\alpha} \sum_s \eta_{\alpha s} \varepsilon(\mathbf{r})_{\alpha s}, \quad (\text{A1})$$

where  $\eta_{\alpha s}$  are the long-range-order parameters and summations are carried out over all stars  $\alpha$  determining the structure and the branches  $s$ ;

$$\begin{aligned} \varepsilon(\mathbf{r})_{\alpha s} = & \frac{1}{2} \sum_{j_{\alpha}} [\gamma(\mathbf{k}_{j_{\alpha}})_s v(p, \mathbf{k}_{j_{\alpha}})_s \exp(i\mathbf{k}_{j_{\alpha}} \mathbf{r}) \\ & + \gamma(\mathbf{k}_{j_{\alpha}})_s^* v(p, \mathbf{k}_{j_{\alpha}})_s^* \exp(-i\mathbf{k}_{j_{\alpha}} \mathbf{r})] \end{aligned} \quad (\text{A2})$$

is the function depending only on the symmetry of the ordered phase rather than on its dynamic properties. The index  $j_{\alpha}$  in (A2) numbers the vectors of the star  $\{\mathbf{k}_{\alpha}\}$ ; the summation in  $j_{\alpha}$  is carried out over all vectors of the star  $\alpha$ . As in the Landau theory,<sup>37</sup> the constants  $\gamma(\mathbf{k}_{j_{\alpha}})_s$  are defined so that

$$\sum_{j_{\alpha}} |\gamma(\mathbf{k}_{j_{\alpha}})_s|^2 = 1, \quad (\text{A3})$$

where the relation between the constants  $\gamma(\mathbf{k}_{j_{\alpha}})_s$  determines the symmetry of the ordered phase. The functions  $\varepsilon(\mathbf{r})_{\alpha s}$  given by (A2) induce irreducible representations of the space group of the disordered phase. Each LRO parameter  $\eta_{\alpha s}$  describing the ordered phase is related to the corresponding irreducible representation of this space group.

To find the atomic structure of a stable ordered phase, we, first, have to find the stars of wave vectors generating the structure and, second, to determine the constants  $\gamma(\mathbf{k}_{j_{\alpha}})_s$ . The vectors  $\{\mathbf{k}_{j_{\alpha}}\}$  of the stars can be found either theoretically, as the ones that minimize the spectrum branch  $\lambda(\mathbf{k})_{-}$ , or experimentally from the diffraction pattern geometry (from the positions of superlattice points in the Brillouin zones of the disordered phase). In the specific case of  $\text{YBa}_2\text{Cu}_3\text{O}_{6+x}$  oxides, the observed diffraction patterns indicate that Eqs. (A1) and (A2) include the wave vectors of the Lifshitz stars  $(000)$ ,  $(\frac{1}{2}\frac{1}{2}0)$ , and  $\{\frac{1}{2}00\}$  and the star  $\{\frac{1}{4}\frac{1}{4}0\}$ .

The coefficients  $\gamma(\mathbf{k}_{j_{\alpha}})_s$ , required for the complete determination of the functions  $\varepsilon(\mathbf{r})_{\alpha s}$  in (A1), can be found from the following criteria which are the necessary conditions of the phase stability.<sup>19,20</sup>

Criterion I. All coefficients  $\gamma(\mathbf{k}_{j_{\alpha}})_s$  entering the functions  $\varepsilon(\mathbf{r})_{\alpha s}$  are the constants within the stability field of the superstructures.

Criterion I demonstrates that the only parameters which are variable within the stability field of a superstructure are the LRO parameters  $\eta_{\alpha s}$ . They are the functions of concentration  $c$  and temperature  $T$ . The coefficients  $\gamma(\mathbf{k}_{j_{\alpha}})_s$  describe the symmetry of the superstructure. To determine the moduli and phases of the nonzero constants  $\gamma(\mathbf{k}_{j_{\alpha}})_s$ , the next criterion can be used.

Criterion II. The constants  $\gamma(\mathbf{k}_{j_{\alpha}})_s$  should be chosen so that total number of different values assumed by the function  $n(p, \mathbf{r})$  on all possible lattice sites  $\{p, \mathbf{r}\}$  should be equal to the number of the LRO parameters  $\eta_{\alpha s}$  in (A1) plus 1.

If criterion I is not trivial and requires an extensive investigation of the free-energy functional using the general symmetry principles, the meaning of criterion II is obvious: it is, in fact, the condition that the number of degrees of freedom in the real lattice representation [a total number of different values assumed by the function  $n(p, \mathbf{r})$  on all lattice sites  $\{p, \mathbf{r}\}$ ] is equal to the total number of degrees of freedom in the reciprocal space representation (the total number of the LRO parameters and composition  $c$ ).

Because the function  $n(p, \mathbf{r})^2$  has the same symmetry

as the function  $n(p, \mathbf{r})$ , it should have exactly the same form (A1) as the function  $n(p, \mathbf{r})$ . The only difference is that, in  $n(p, \mathbf{r})^2$  we have the functions  $\bar{\eta}(\dots \eta_{\alpha s}, \dots, c)$  and  $\bar{c}(\dots \eta_{\alpha s}, \dots, c)$ , instead of the coefficients  $\eta_{\alpha s}$  and  $c$ . Verification of the fact that the functions  $n(p, \mathbf{r})^2$  and  $n(p, \mathbf{r})$  have the same form (with accuracy to the coefficients  $\eta_{\alpha s}$  and  $c$ ) can be obtained by squaring Eq. (A1). It is actually an additional test for correctness of

the choice of  $\gamma(\mathbf{k}_{j\alpha})_s$ . All the distributions  $n(p, \mathbf{r})$  presented in this paper meet these stability criteria.

Finally, it should be emphasized that the above method of the ordered structure determination is actually based on the quite general symmetry consideration and is valid irrespective of the approximation of the system dynamics.

- <sup>1</sup>S. Semenovskaya and A. G. Khachatryan, Phys. Rev. B **46**, 6511 (1992); Physica D **66**, 205 (1993).
- <sup>2</sup>Th. Zeiske, D. Hohlwein, R. Sonntag, F. Kubanek, and G. Collin, Z. Phys. B **86**, 11 (1992).
- <sup>3</sup>Tan Kemin, Hu Meisheng, and W. Yening, J. Phys. Condens. Matter **1**, 1049 (1989).
- <sup>4</sup>G. Van Tendeloo, H. W. Zanderbergen, and S. Amelinckx, Solid State Commun. **63**, 289 (1987); **63**, 609 (1987).
- <sup>5</sup>D. J. Werder, C. H. Chen, R. J. Cava, and B. Batlogg, Phys. Rev. B **37**, 2317 (1988).
- <sup>6</sup>R. Beyers, B. T. Ahn, G. Gorman, V. Y. Lee, and S. S. P. Parkin, M. L. Ramirez, K. P. Roche, J. E. Vazquez, T. M. Gur, and R. A. Huggins, Nature **340**, 6235 (1989).
- <sup>7</sup>J. Reyes-Gasga, T. Krekels, G. Van Tendeloo, J. Van Landuyt, S. Amelinckx, W. H. M. Bruggink, and H. Wergweij, Physica C **159**, 831 (1989).
- <sup>8</sup>S. Yang, H. Claus, B. W. Veal, R. Wheeler, A. P. Paulikas, and J. W. Downey, Physica C **193**, 243 (1992).
- <sup>9</sup>M. A. Alario-Franco, C. Chaillout, J. J. Capponi, and J. Chenavas, Mater. Res. Bull. **22**, 1685 (1987).
- <sup>10</sup>M. A. Alario-Franco, J. J. Capponi, C. Chaillout, and J. Chenavas, Mater. Res. Soc. Symp. Proc. **99**, 41 (1988).
- <sup>11</sup>M. A. Alario-Franco, C. Chaillout, J. J. Capponi, J. Chenavas, and M. Marezio, Physica C **156**, 455 (1988).
- <sup>12</sup>C. Chaillout, M. A. Alario-Franco, J. J. Capponi, J. Chenavas, J. L. Hodeau, and M. Marezio, Phys. Rev. B **36**, 7118 (1987).
- <sup>13</sup>R. Sonntag, D. Hohlwein, T. Brucke, and G. Collin, Phys. Rev. Lett. **66**, 1497 (1991).
- <sup>14</sup>T. Krekels, T. S. Shi, J. Reyes-Gasga, G. Van Tendeloo, J. Van Landuyt, and S. Amelinckx, Physica C **167**, 677 (1990).
- <sup>15</sup>D. J. Werder, C. H. Chen, and G. P. Espinosa, Physica C **173**, 285 (1991).
- <sup>16</sup>C. N. R. Rao, R. Nagarajan, A. K. Ganguli, G. N. Subbanna, and S. V. Bhat, Phys. Rev. B **42**, 6765 (1990).
- <sup>17</sup>R. Sonntag, Th. Zeiske, and D. Hohlwein, Physica B **180-181**, 374 (1992).
- <sup>18</sup>R. J. Cava, A. W. Hewat, E. A. Hewat, B. Batlogg, M. Marezio, K. M. Rabe, J. J. Krajewski, W. F. Peck, Jr., and L. W. Rupp, Jr., Physica C **165**, 419 (1990).
- <sup>19</sup>A. G. Khachatryan, Phys. Status Solidi B **60**, 9 (1973); Sov. Phys. JETP **36**, 753 (1973).
- <sup>20</sup>A. G. Khachatryan, *The Theory of Structural Transformation in Solids* (Wiley, New York, 1983).
- <sup>21</sup>Z. Hiroi and M. Tokano, Solid State Commun. **65**, 1549 (1988).
- <sup>22</sup>A. A. Aligia, J. Garces, and H. Bonadeo, Physica C **190**, 234 (1992).
- <sup>23</sup>J. D. Jorgensen, B. W. Veal, A. P. Paulikas, L. J. Nowicki, G. W. Crabtree, H. Claus, and W. K. Kwok, Phys. Rev. B **41**, 1863 (1990).
- <sup>24</sup>Th. Zeiske, R. Sonntag, D. Hohlwein, N. H. Andersen, and T. Wolf, Nature **353**, 542 (1991).
- <sup>25</sup>A. G. Khachatryan and J. W. Morris, Jr., Phys. Rev. Lett. **61**, 215 (1988); **64**, 76 (1990).
- <sup>26</sup>W. Schwartz, O. Blaschko, G. Collin, and F. Maruccio, Phys. Rev. B **48**, 6513 (1993).
- <sup>27</sup>L. E. Levine and M. Daumling, Phys. Rev. B **45**, 8146 (1992).
- <sup>28</sup>S. Semenovskaya and A. G. Khachatryan, Phys. Rev. Lett. **67**, 2223 (1991).
- <sup>29</sup>S. Semenovskaya and A. G. Khachatryan, Philos. Mag. Lett. **66**, 105 (1992).
- <sup>30</sup>A. A. Aligia, J. Garces, and H. Bonadeo, Phys. Rev. B **42**, 10226 (1990).
- <sup>31</sup>Ming Lei, J. L. Sarrao, W. M. Visscher, T. M. Bell, J. D. Thompson, A. Migliori, U. W. Welp, and B. Veal, Phys. Rev. B **47**, 6154 (1993).
- <sup>32</sup>J. D. Jorgensen, M. A. Beno, D. G. Hinks, L. Soderholm, H. J. Volin, R. L. Hitterman, J. D. Grace, I. K. Schuller, C. V. Serge, K. Zhang, and M. S. Kleefish, Phys. Rev. B **36**, 3608 (1987).
- <sup>33</sup>B. W. Veal, A. P. Paulikas, H. You, Y. Fang, and J. W. Downey, Phys. Rev. B **42**, 6305 (1990).
- <sup>34</sup>A. A. Aligia and J. Garces, Phys. Rev. B **49**, 524 (1994).
- <sup>35</sup>D. Adelman, C. P. Burmester, L. T. Willi, P. A. Stern, and R. Gronsky, J. Phys. Condens. Matter **4**, L585 (1992).
- <sup>36</sup>V. Plakhty, A. Stratilatov, Yu. Chernenkov, V. Fedorov, S. K. Sinha, C. L. Loong, B. Gaulin, M. Vlasov, and S. Moshkin, Solid State Commun. **84**, 639 (1992).
- <sup>37</sup>L. D. Landau and E. M. Lifshitz, *Statistical Physics* (Pergamon, New York, 1980), Part 1.

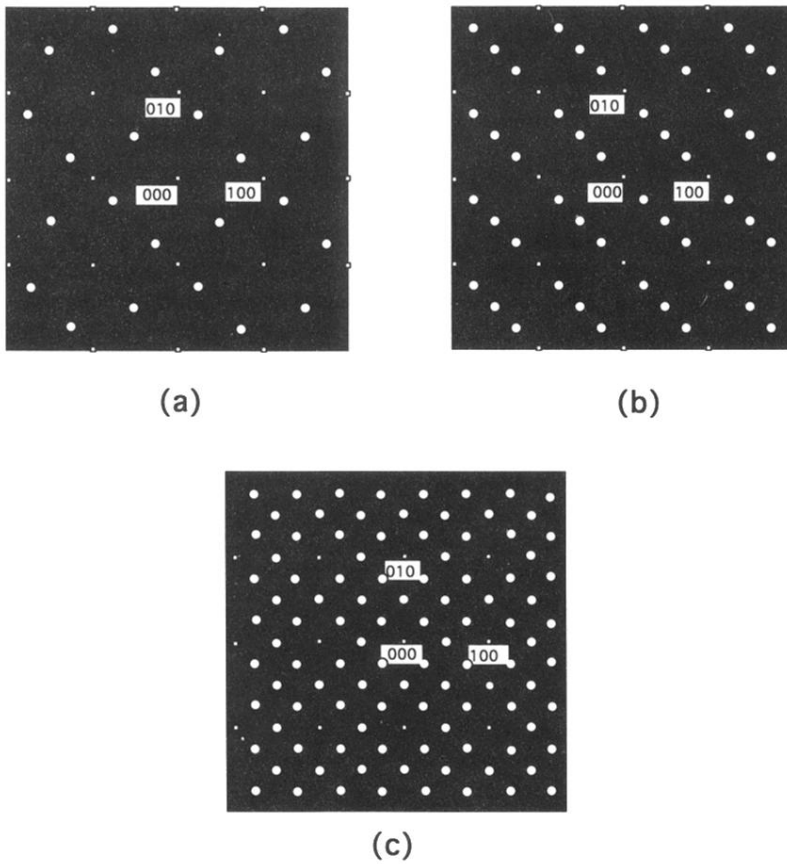


FIG. 1. Schematic presentation of three types of observed  $(HK0)$  diffraction patterns for the  $\{\frac{1}{4}\frac{1}{4}0\}$  phases in the  $\text{YBa}_2\text{Cu}_3\text{O}_{6+x}$  system: (a) x-ray diffraction from the  $\sqrt{2}a_0 \times 2\sqrt{2}a_0$  structure observed by Zeiske *et al.* (Ref. 2) from a single orientation variant of  $\text{YBa}_2\text{Cu}_3\text{O}_{6.35}$  ( $x=0.35$ ); (b) the diffraction pattern of another  $\sqrt{2}a_0 \times 2\sqrt{2}a_0$  structure observed by Kemin *et al.*; (c) the most frequently observed diffraction for the  $2\sqrt{2}a_0 \times 2\sqrt{2}a_0$  structure (Refs. 7, 10–12, 14, 15, and others). The superstructure maxima are shown by large circles, the fundamental reflections by small points (indices of three fundamental reflections are marked).

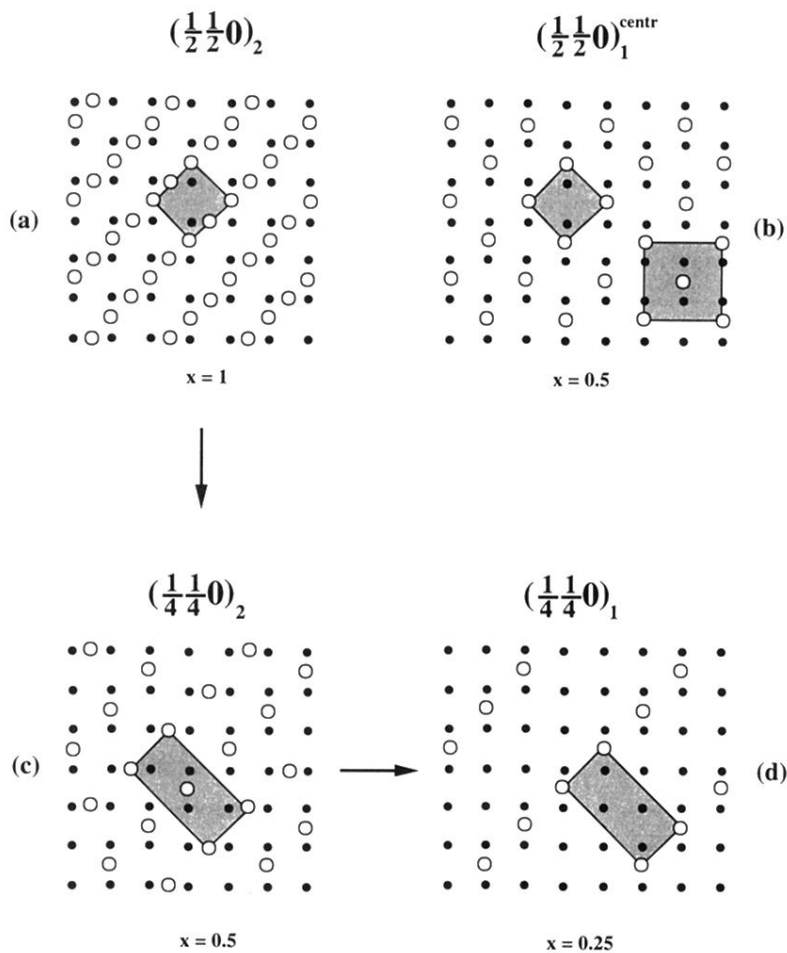


FIG. 2. The [110] oxygen chain superstructures (a)–(d) at  $x < \sim 0.35$ , generated by the  $(\frac{1}{2} \frac{1}{2} 0)$  Lifshitz star. The structures are described by Eqs. (1a), (1b), (2a), and (2b), respectively. The  $(\frac{1}{4} \frac{1}{4} 0)_2$  (c) and  $(\frac{1}{4} \frac{1}{4} 0)_1$  (d) are the secondary and tertiary ordered structures with a  $\sqrt{2}a_0 \times 2\sqrt{2}a_0$  unit cell. Their diffraction patterns are shown in Figs. 1(a) and 1(b). The transitions order [sequence (3) or (22c)] upon cooling is shown by arrows.

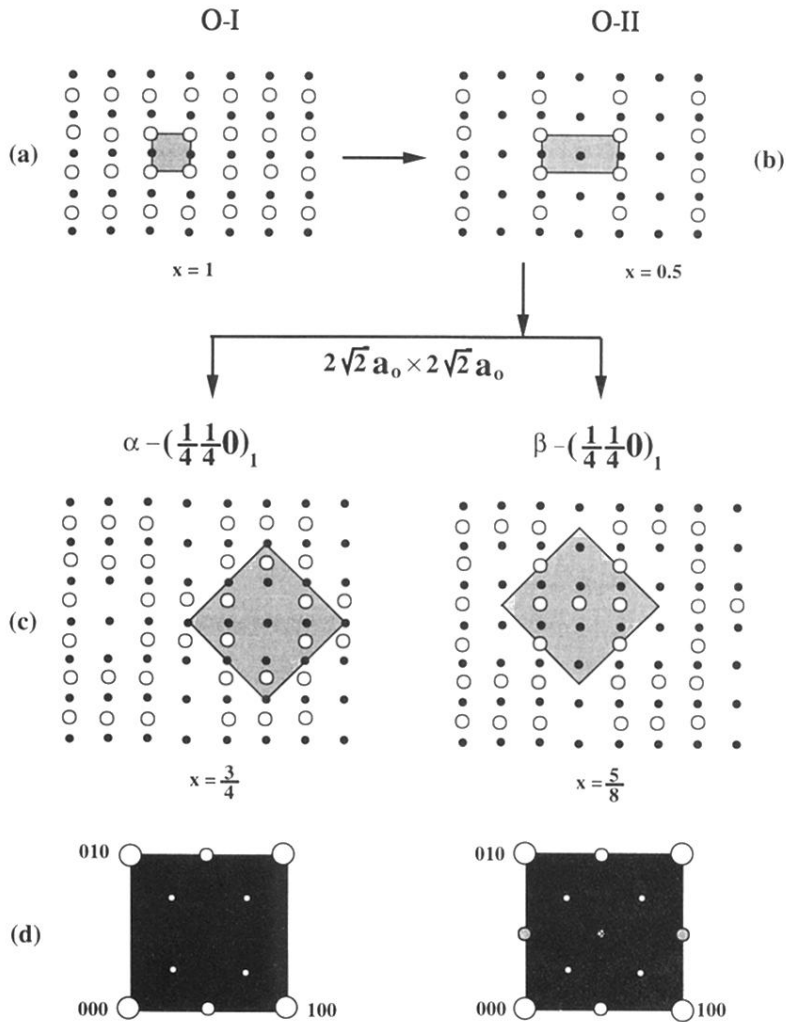


FIG. 3. The [010] Cu-O chain superstructures (with corresponding stoichiometries  $x$ ) generated by the (000) Lifshitz star at  $x > \sim 0.4-0.45$ . The observed O-I and double-period O-II ordered structures correspond to the Lifshitz points (000) and  $\{\frac{1}{2}00\}$ . The  $\alpha - (\frac{1}{4} \frac{1}{4} 0)_1$  and  $\beta - (\frac{1}{4} \frac{1}{4} 0)_1$  phases (c) with a  $2\sqrt{2}a_0 \times 2\sqrt{2}a_0$  unit cell are the tertiary ordered superstructures of the secondary ordered O-II phase. Their diffraction patterns are shown in (d). The transitions order [sequence (4) or (22a)] upon cooling is shown by arrows.

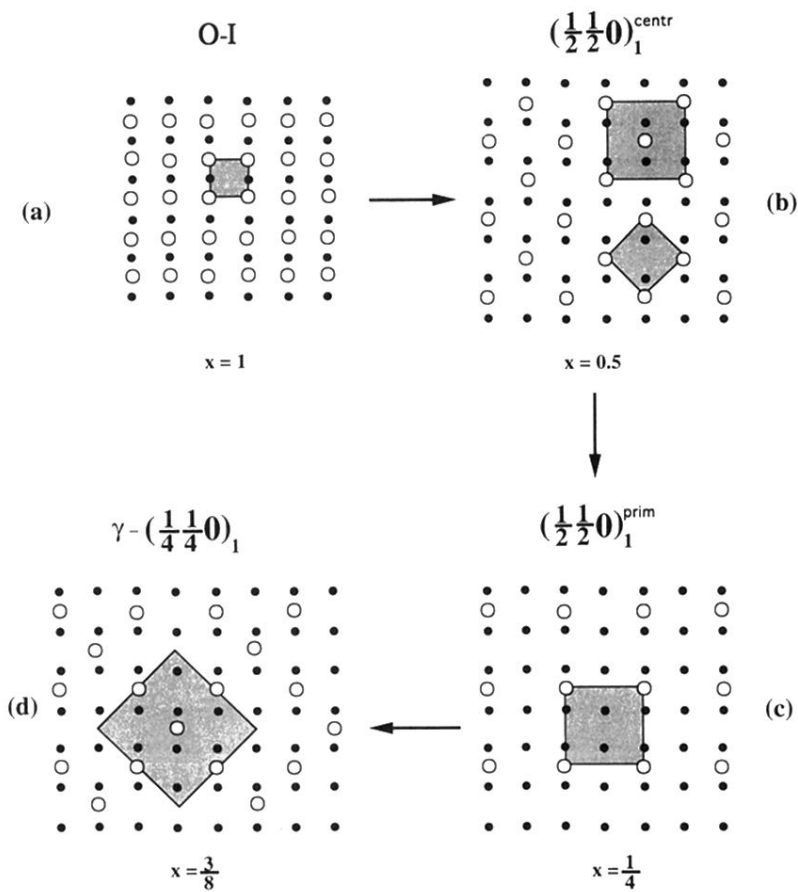


FIG. 5. The family of orthorhombic superstructures, described by Eqs. (17), (1b), (18), and (19) [the structures (a)–(d), respectively] which are the derivatives of the O-I phase within the intermediate range  $\sim 0.35 < x < \sim 0.4$ . The  $(\frac{1}{2}\frac{1}{2}\mathbf{0})_1^{\text{prim}}$  phase (c) was observed (Ref. 7) as a precursor of the  $\gamma-(\frac{1}{4}\frac{1}{4}\mathbf{0})_1$  ( $2\sqrt{2}a_0 \times 2\sqrt{2}a_0$ ) phase (d). The diffraction of the  $\gamma-(\frac{1}{4}\frac{1}{4}\mathbf{0})_1$  ( $2\sqrt{2}a_0 \times 2\sqrt{2}a_0$ ) phase [Fig. 1(c)] was found in Refs. 7 and 13.